IEEE Access
Multidisciplinary | Rapid Review | Open Access Journal

Received March 4, 2021, accepted March 12, 2021, date of publication March 23, 2021, date of current version March 30, 2021.

Digital Object Identifier 10.1109/ACCESS.2021.3068116

Simulation and Measurement Data-Based Study on Fat as Propagation Medium in WBAN Abdominal Implant Communication Systems

MARIELLA SÄRESTÖNIEMI[1], (Member, IEEE), CARLOS POMALAZA-RÁEZ[2], (Senior Member, IEEE), CHAÏMAÂ KISSI[3], AND JARI IINATTI[1], (Senior Member, IEEE)

[1]Centre for Wireless Communications, Faculty of Information Technology and Electrical Engineering, University of Oulu, 90014 Oulu, Finland
[2]Department of Electrical and Computer Engineering, Purdue University, Fort Wayne, IN 46805-1499, USA
[3]Electronics and Telecommunication System Research Group, National School of Applied Sciences (ENSA), Ibn Tofail University, Kenitra 14000, Morocco

Corresponding author: Mariella Särestöniemi (mariella.sarestoniemi@oulu.fi)

This work was supported in part by the projects WBAN Communications in the Congested Environments (MeCCE), in part by the Academy of Finland 6Genesis Flagship under Grant 318927, and in part by the European Union's Horizon 2020 programme through the Marie Sklodowska-Curie Grant under Agreement 872752.

ABSTRACT This paper presents comprehensive study on fat as propagation medium in abdominal implant communication system at low ultrawideband (UWB) frequency range 3.75-4.25 GHz. The main aim is to investigate how signal propagates through visceral and subcutaneous fat layers and how that information can be exploited in implant communication systems. The study is conducted using different methods: electromagnetic simulations, power flow analysis, propagation path calculations and radio channel measurements with animal meat pieces. Simulations are conducted using layer models and anatomical voxel models having different sizes. Results of channel simulations are verified with propagation path calculations. Power flow analysis on cross-cuts of the voxel models is conducted to investigate how the signal propagates inside the tissues. Furthermore, measurements using different animal meat pieces are performed to evaluate the impact of fat constitution on channel characteristics. It is found that similar tendency on fat propagation is seen in the evaluations with different methods. It is also observed that channel attenuation depends not only on the types and thicknesses of the tissues between transmitter and receiver antennas, but also how the tissues, especially fat, is located between the antennas. Channel attenuation difference between different voxels is maximum 14 dB in the studied antenna locations. Furthermore, propagation channel is evaluated with measurements using pork meat having different fat and muscle constitutions. It is found that antenna location respect to fat layers has clear impact on the channel strength although the fat tissue is not directly above the in-body antenna. The difference is noted to be 3-15 dB especially on the side peaks of channel impulse response. The knowledge on fat as a propagation medium is crucial when designing medical monitoring or implant communication systems. Location of antennas/sensor nodes for the monitoring devices can be established so that propagation through fat layer can be exploited.

INDEX TERMS Anatomical voxel model, capsule endoscopy, directive antenna, finite integration technique, gastrointestinal monitoring, implant communications, power distribution, radio channel, wireless body area networks.

I. INTRODUCTION

Medical implant communications and in-body propagation have been intensively studied topics for Wireless Body Area Network (WBAN) applications for several years [1]–[29]. Different techniques are evaluated to transmit the data from the implant to the on-body device. Ultra wideband (UWB) has become an attractive alternative for the communication link since it enables reliable and high-data rate data transfer with low power consumption and simple electronics. This is favorable feature especially for capsule endoscopy in which high resolution pictures should be transferred reliably [6]–[9]. Previously, UWB range was considered unrealistic for capsule endoscopy since the propagation losses in the

The associate editor coordinating the review of this manuscript and approving it for publication was Chan Hwang See.

tissues increase as the frequency increases. However, recently the lower part of the UWB band is considered suitable for the capsule endoscopy applications especially if directive on-body antennas are used [7] and thus, several in-body propagation studies at lower UWB frequency ranges have been presented in the literature [8]–[16].

One important result in the in-body propagation studies is that the fat tissue is an excellent propagation medium compared to the other human tissues [16], [22]–[29] in terms of propagation loss and propagation speed since its relative permittivity is clearly lower than e.g. in muscle tissue [30], [31]. Pioneering work in fat propagation research was done by *Asan et al*. in few recent papers [23]–[25], in which fat as propagation medium was studied with layer model simulations as well as ex-vivo pork and phantom measurements. The studies were conducted at ISM frequency band 2.45 GHz. The studies show how signal transmission improves as the thickness of the fat layer is increased respect to the muscle layer in the layer model. *Asan et al*. extended further the fat channel studies for data packet transmission evaluations [26], effect of thickness inhomogeneity [27], and for the presence of blood vessels in fat tissue [28], [29].

Beneficial properties of fat as propagation channel, fast signal propagation with low propagation losses, were presented with anatomical voxel models for the first time by *Särestöniemi et al* in [16], which presents power distribution studies for the abdominal monitoring systems at 3.75-4.25 GHz. This study focused only on general power distribution studies in the abdominal tissues pointing out the phenomenon of smooth propagation through the fat layer, detailed study of fat as propagation medium was out of the scope. Additionally, radio channel evaluations between the capsule endoscope and the on-body antennas presented in [8], [9] further verified the impact of the vicinity of fat paths on the channel strength. Also, in these studies, fat as propagation medium was not the scope of the study. Instead, *Särestöniemi et al*. focused on propagation through fat later in [22] in which the anatomical voxel simulation results were compared with the *on-body* measurement results with volunteers of different sizes and body constitutions. The results were further verified with propagation path calculations. These evaluations were done with two on-body antennas, between which the signal propagates on the body surface as well as inside the body through the fat layers. It was shown that although the other antenna is placed in the middle of the abdomen and the other one on the flank, clear power flow propagates though the fat layers inside the body. Furthermore, the author has presented in-body propagation studies with different pork meats [32]. The study showed how the meat constitution has significant impact on the in-body channel: the propagation loss in meat with interlaced muscle and fat tissues have is significantly lower channel attenuation than that in the meat with separate muscle and fat layers.

This paper extends previous studies on fat propagation by evaluating how the signal propagates through the visceral and subcutaneous fat layers between the implant and the on-body antenna. The study is conducted by applying a comprehensive set of methods: electromagnetic simulations, ex-vivo animal meat measurements, and propagation path calculations. Likewise in author's previous studies, the selected frequency band is 3.75-4.25 GHz, which is the mandatory channel in UWB implant communications in the IEEE 802.15.6 standard [5]. The research is carried out by evaluating propagation between an abdominal implant and a directive on-body antenna using anatomical voxel models, different layer models, power flow analysis, radio channel in-body measurements with pork meat, as well as propagation path calculations. Even though an endoscope capsule is used, the idea can be extended to any other abdominal implant communication system, e.g. for gastrointestinal track activity monitoring systems.

The novelty of this research is to present a comprehensive study on the fat as propagation medium in implant communications at 4 GHz range using several anatomical voxel models having different sizes and body constitutions. Other studies have not verified the results of fat propagation studies with propagation path calculations together with animal meat measurements results. Furthermore, the impact of the antenna locations (both in-body and on-body) respect to the fat layers has not been studied earlier both with simulations and the measurements.

This paper is organized as follows: Section II presents the study cases describing the simulations, measurements, and antennas used in this study. Furthermore, Section III presents 2D power flow studies both for implant antenna and on-body antenna. Section IV presents simulation results obtained with layer models and voxel models as well as verifies the results with propagation path calculations. Section V presents channel evaluations using different set of animal meats. Section VI discusses comprehensively the simulation and measurement results and considers their impact and correspondence. Summary and Conclusions are given in Section VII. Section VIII presents discussion and analyses the impact of the results as well as depicts some future work directions.

II. STUDY CASE

A. ANTENNAS

In this study, we use a directive on-body antenna designed for in-body communications for low-UWB frequency range 3.75 – 4.25 GHz. The antenna, illustrated in Fig. 1a, was originally presented in [33] and is further used in several in-body channel studies in [8], [9], [16], [22], [32]–[35]. The dimensions of the antenna without and with the cavity are 2.5 cm × 2.5 cm and 9 cm × 14 cm, respectively. The on-body realized gain at 4 GHz and the on-body return loss of this antenna are presented in Figs. 1b-c, respectively.

As an in-body antenna, we use two different omni-directional antennas. The first antenna, illustrated in Fig. 1d, is a small omni-directional dipole antenna embedded inside a realistic size plastic capsule shell (Fig. 1e), which has been used in our capsule endoscope studies [8], [9], [16]. The gain at 4 GHz and return loss, both simulated inside the small

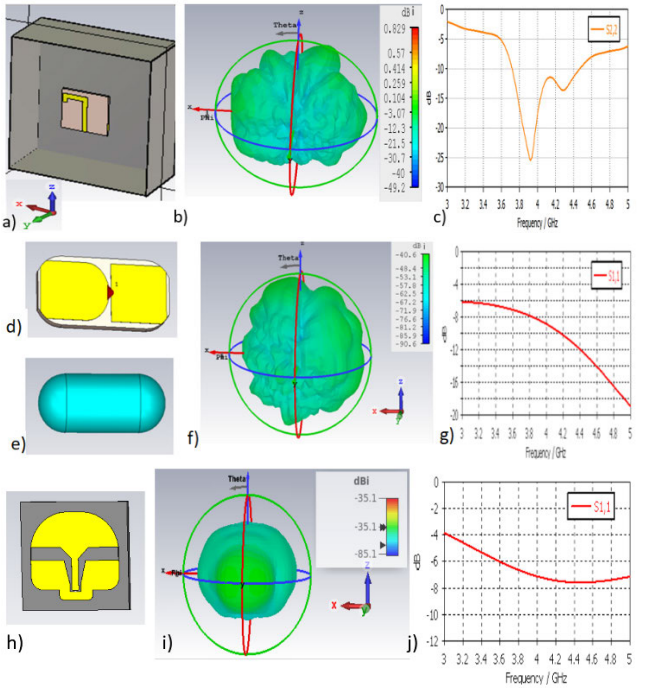

FIGURE 1. The low-UWB on-body antenna's a) structure, b) realized gain at 4 GHz, c) return loss; Capsule antenna's d) structure, e) capsule shell, f) realized gain at 4 GHz, g) return loss; Loop antenna's h) structure, i) realized gain at 4 GHz, and j) return loss.

intestine (SI) tissue, are presented in Fig. 1f-g, respectively. More details of the antenna can be found in [8], [9].

The second omni-directional antenna, which was originally designed for on-body communications [36] but which is used to resemble the second in-body antenna in our fat propagation studies, is illustrated in Fig. 1h. This loop antenna is originally designed to cover whole UWB band 3.1-10.6 GHz and it has been used in several on-body studies e.g. in [33], [34]. In [32], we used loop antenna in pork meat in-body measurements since it has shown to provide similar channel behavior as the first in-body antenna and since the prototype of the first in-body antenna was not available [32]. The loop antenna's in-body realized gain at 4 GHz and return loss are presented in Figs. 1 i-j, respectively.

B. SIMULATIONS

Simulations are carried out with the electromagnetic simulation software Simulia CST Studio Suite [37] which is based on finite integration technique (FIT). CST provides complex channel parameter S21, which is further converted into the time domain with Inverse Fast Fourier transform (IFFT) in Matlab to obtain channel impulse response (IR) for the selected bandwidth. The simulations were conducted for the frequency band 0.5-5 GHz and IFFT was performed for the frequency range 3-5 GHz. The samples of frequency range 0.5-3 GHz were left out of the IFFT as none of the antennas work at that frequency range. The loop antenna is originally designed for the UWB range 3.1-10.6 GHz and the capsule antenna is also working reasonably at 3-5 GHz. Thus,

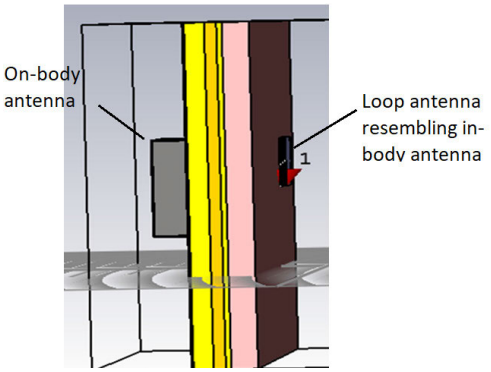

FIGURE 2. Layer model with on-body antenna and in-body antenna 2.

IFFT length is increased from on-body antenna's operational bandwidth 3.75-4.25 GHz to 3-5 GHz to increase resolution in time domain.

The default input power in the CST simulations is 0.5 W which can be modified to meet safety requirement respect to the Specific Absorption Ratio (SAR)-values for each antenna and study case. However, our study includes only evaluations of parameters that depend on the ratio of input and output powers and thus, the CST default input power could be used.

Simulations are conducted using layer models as well as CST's anatomical voxel models. The layer model is illustrated in Fig. 2 and its dimensions are presented in Table 1. The layer model is further modified for different fat propagation studies, these modifications are explained in Section III.

TABLE 1. Thickness of the tissues in the layer model and dielectric properties of tissues.

Tissue	Thickness [cm]	Permittivity	Wavelength [λ] at 4 GHz
Skin	0.2	36.6	0.012
Subcutaneous fat	1.0	5.12	0.033
Muscle	1.5	50.8	0.010
Visceral fat	0.3	5.12	0.033
Small intestine	1.5	51.6	0.010

CST provides several voxel models, among which we selected anatomical voxel models Laura, Donna, and Gustav, presented in Fig. 3a-c. Laura corresponds to a lean female body with resolution of 1.88 mm × 1.88 mm × 1.25 mm. Gustav is a normal-weighted male with the resolution of 2.08 mm × 2.08 mm × 2 mm. Donna resembles overweight middle-aged female with resolution of 1.88 mm × 1.88 mm × 1.25 mm. The lines in the figures depict the area where the implant antenna is located and where the cross-cut is performed for the voxel model. For Laura and Donna, the cross-cut is performed on the navel area, since their small intestines are located on the front part of the abdomen. Instead for Gustav, who is taller than the other models, small intestine is located on the front part of the abdomen slightly above the navel area.

Cross-sections of these models are presented in Figs. 4a–c. As it is noted, there are clear differences in the structures of

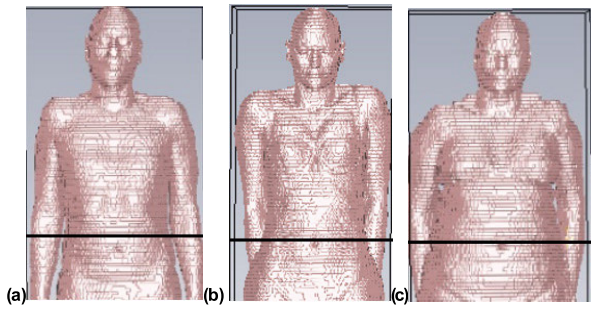

FIGURE 3. Voxel models used in this study: a) Gustav, b) Laura, and c) Donna.

the intestine area between the models. Besides, thicknesses of the fat layers (both inner and outer) and muscle layer vary significantly between the models. The implant antenna location in each model is depicted in figures as well.

CST creates automatically mesh in the simulation in a way that mesh is denser in the areas where the structure is more complex. The mesh view on the capsule antenna region is presented in Fig. 5. As one can note, the mesh is very dense inside the voxel model, especially in the capsule antenna location and particularly in the antenna port region (vertical red line). The mesh is significantly denser than the voxel's pixel size and hence the obtained results can be considered to be realistic.

Computational complexity of voxel simulations in CST is huge since the number of mesh cells is enormous even in the cut torso. For the torsos of Gustav, Laura and Donna, number of mesh cells is approximately 400 million whereas with the layer model that is only 20 million. High number of the mesh cells in the voxel models is due to the anatomical accuracy. Such huge models require large computational capacity. These simulations were carried of out as parallel processing of six cluster nodes with Inter(R) Xeon(R) CPU E5-2640 v4.

C. PORK MEAT MEASUREMENTS

The measurements were conducted at the University of Oulu by using an Agilent 8720ES vector network analyzer (VNA), 1.5 m coaxial cables, as well as the prototypes of the low-UWB on-body antenna and the loop antenna having SMA connectors presented in Figs. 6a-b. More details about the antennas and the prototypes can be found in [33] and [36]. The proper calibration of VNA was conducted before the measurements to eliminate loss due to cables etc.

The measured frequency range was 2-10.6 GHz covering the full UWB band 3.1-10.6 GHz since the loop antenna is designed for that frequency range and wider frequency band increases resolution in time domain. The measurements were conducted in the frequency domain to obtain radio channel frequency responses S21 parameters, which were converted into time domain by performing IFFT for 2-5 GHz band. The input power in the measurements was 0.0032 W.

For these in-body propagation studies, we used two different pork meat pieces: *Meat1* and *Meat2*, which are depicted in Figs. 7a-b. Besides, we used beef minced meat having different fat percentages: 10%, 15%, and 20% and which are presented in Figs.7c-e. More details can be found in Section IV where the measurement study and results are explained.

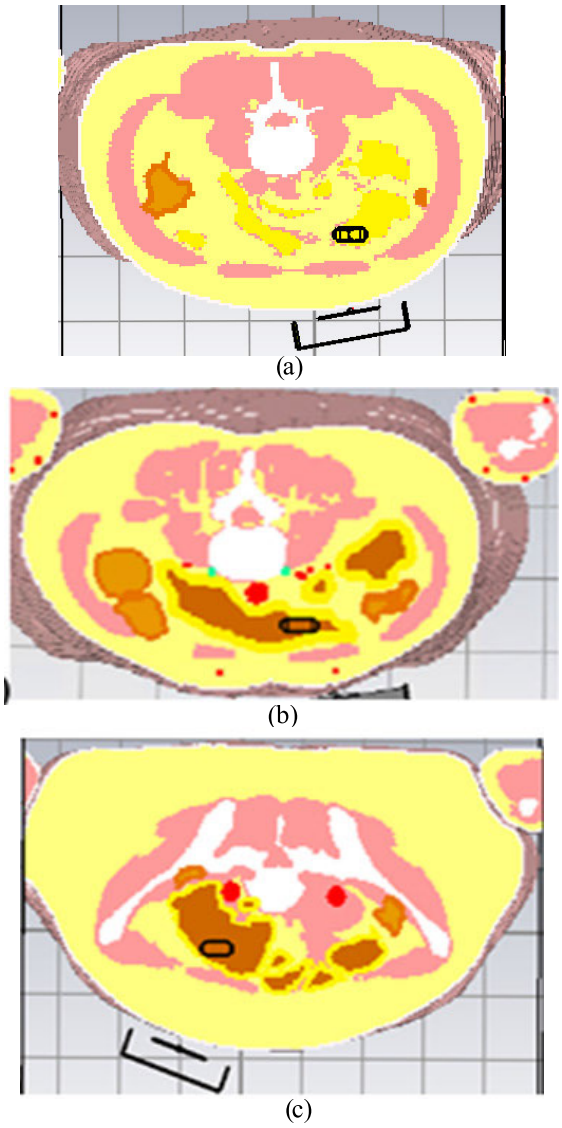

FIGURE 4. Cross-cuts of the voxel models a) Gustav, b) Laura, and c) Donna.

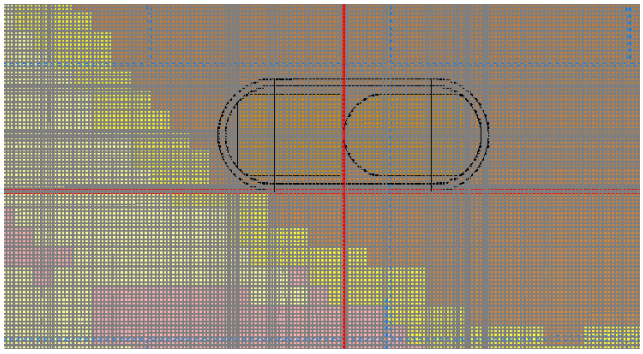

FIGURE 5. Mesh view on the capsule antenna inside the voxel model.

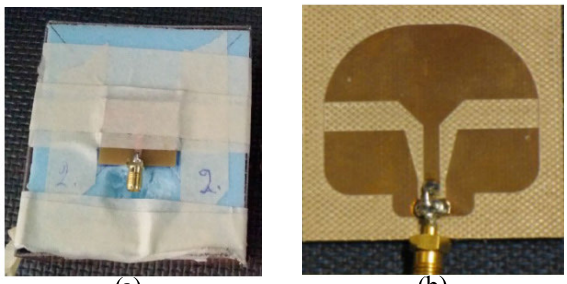

FIGURE 6. a) low-UWB antenna prototype [33], b) loop antenna prototype [36].

The meat pieces were set individually inside a cubicle made by absorber pieces to avoid signal interference from the surrounding environment as well as minimize the propagation overflow from the sides of meat pieces. The antennas, which were placed on the top and below the meat piece, were connected to the VNA's ports with coaxial cables, as presented by the measurement setup diagram in Fig. 8a. The meat piece was set inside a thin plastic bag to protect the antennas and the absorbers. The picture of the measurement setup before positioning the antennas on the top and below of the meat piece is presented in Fig. 8b [32]. Different subjects in the measurement setup are indicated with colored pointers. Temperature meter was used to verify that the meat temperature is same for all meat pieces (+12'C, the temperature meter was removed before starting the channel measurements). More details on similar measurements with pork meat can be studied in [32].

III. 2D POWER FLOW REPRESENTATION

The propagation through the subcutaneous and the visceral fat layer is studied via power flow representations. Power flow at one frequency represents the real part of complex Poynting vector [38]. It gives instantaneous value at certain (x, y, z) points, as described e.g. in [35]. In this study, the power flow unit is expressed as decibels, normalized so that 0 dB is at its maximum, i.e. at the transmitting antenna.

Arrow-based power flow representation is used since arrows show clearly the direction of the power flow within the tissues and hence visualize the diffraction occurred in the tissue borders. Firstly, the power flow is studied from the capsule which is located inside the small intestine. Secondly, the power flow is studied at the antenna location 1 to observe the propagation through the fat layers as the transmitting antenna is on the navel, which is considered on of the best on-body antenna location for implant communications [16].

A. CAPSULE ANTENNA POWER FLOW

1) HORIZONTAL CROSS-CUT

In this subsection, power flow from the capsule antenna is studied. The power flow representations on the horizontal cross-cut of Laura voxel is presented for dB range −80–0 dB in Fig. 9. The radiation pattern of the capsule antenna is omni-directional except on the gables of the capsule, as presented in [16]. This can be seen also as the strongest

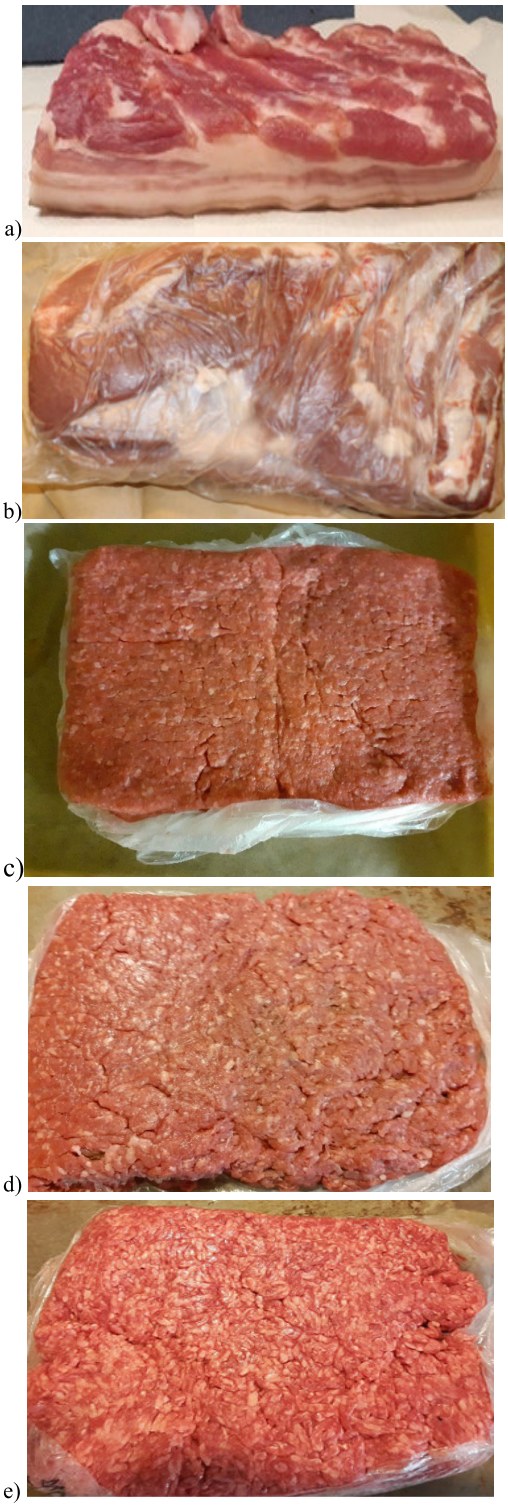

FIGURE 7. Meat samples used in the measurements: a) *Meat1* (pork), b) *Meat2* (pork), as well as beef minced meats with different fat percentages c) 10%, d) 15%, and e) 20%.

power flows from the sides of the capsule. Besides of power spreading according to antennas radiation pattern, there is a clear power flow seen in visceral and subcutaneous fat layers. Within the determined dB range, the signal can reach almost the flank areas due to strong power flow in the outer fat layer.

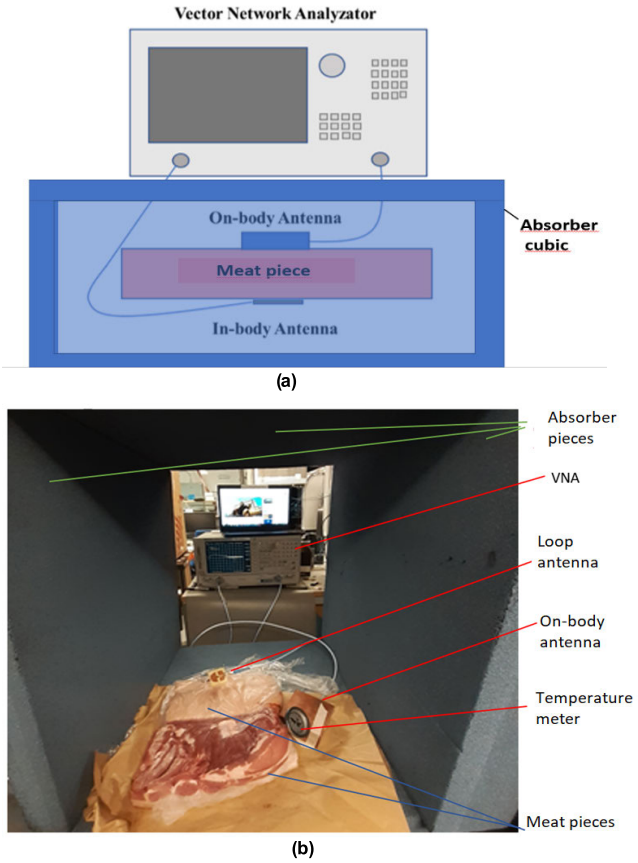

FIGURE 8. a) Measurement setup diagram, b) picture of the measurement setup before positioning the antennas on top and below the meat piece and without closing the back and front walls.

TABLE 2. Power flow at different locations in horizontal cross-cut.

Location	A	B	C	D	E
Power [dB]	0	-18	-30	-35	-56

Interestingly, both left and right flanks are reached almost equally though the capsule itself is located more on the right side of the body. This is due to the abdominal central line, the gap between the abdominal muscle layers, which facilitates propagation towards the left flank as well. Moreover, one can note a strong power flow though the visceral fat towards the inner parts of the body reaching almost the back muscles.

Next, the power values around the capsule area in the fat layers are compared to the power values at equal distance in the muscle tissues. The locations are presented in Fig. 9b, which is a zoomed version of Fig. 9a. The location 'A' refers to capsule location inside the small intestine, the location 'B' is in the visceral fat layer 2 cm from the from the capsule towards the inner body part, and the location 'C' is in the muscle tissue 2 cm from the capsule towards the outer body part. The locations 'B' and 'C' are on the area towards which the strongest power flow travels according to the radiation pattern. Besides, the power flow is evaluated at locations 'D' and 'E', which are on the zone of weaker propagation flow

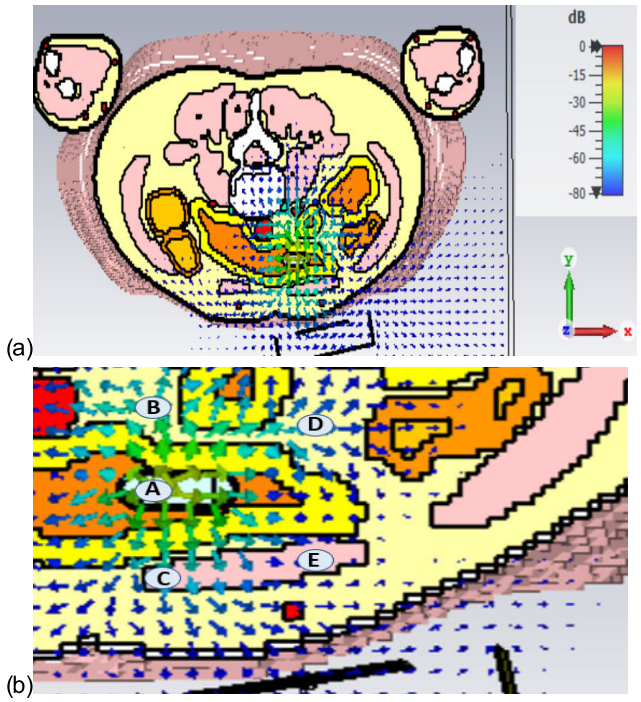

FIGURE 9. Power flow at 4 GHz on the cross-cut of Laura-voxel model: a) whole cross-cut with dB range 0 - −80 dB, b) zoomed version with locations where power is evaluated, dB range 0 - −65 dB.

since they are located closer to the gable of the capsule where radiation is weaker. 'D' is also in the fat tissue and 'E' in the middle of muscle tissue. The powers at these locations are summarized in Table 2.

Power loss from the capsule to the location 'B' is −18 dB whereas power loss from the capsule to the location 'C' is −35 dB. The radiation pattern of the antenna is similar towards both direction and hence, the power difference is due to the tissues through which the signal needs to travel before reaching the determined location. For the location 'B', the signal travels though the small intestine wall and then through the fat layer. Instead, for the location 'C', it needs to travel thought the small intestine content, small intestine wall and the muscle tissue, all of these are difficult propagation medium at 4 GHz as shown in Table 1.

The power difference is even more remarkable in the area where the antenna gain is weaker, i.e. in the locations 'D' and 'E', in which the power is −35 dB and −56 dB, respectively. The power is higher in the location 'D' because it is in the middle of wider visceral fat area towards which the power flows through the thin fat area between two intestine areas. For instance, the radiation from the capsule towards the inner part of the body partly experiences diffraction when hitting the inner small intestine area. These diffracted components turn towards the location 'D' which explains clearly higher power level. Instead, in the location E, though it has exactly same physical distance from the capsule as 'D', the power is at roughly 20 dB lower level. This can be understood by studying the directions of the power flow arrows in Fig.7b: The abdominal muscle layer on the right is a large obstacle

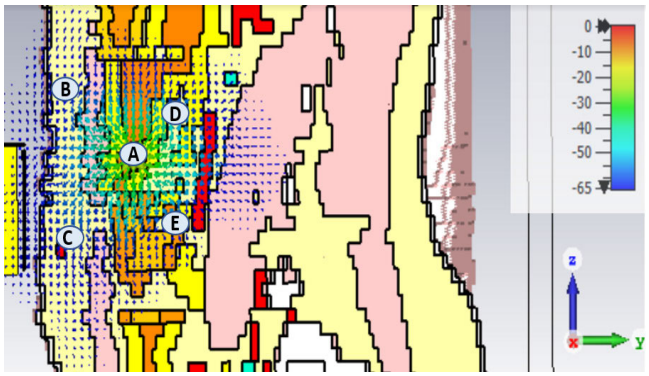

FIGURE 10. Power flow at 4 GHz in the vertical cross-cut of Laura voxel with locations 'A'-'E' where the power is evaluated.

TABLE 3. Power flow at different locations in vertical cross-cut.

Locations	A	B	C	D	E
Power [dB]	0	-51	-38	-31	-38

for the propagation from the capsule towards outer part of the body. Especially in the area towards to the capsule gable, plenty of power is diffracted when hitting the muscle tissue and thus the power inside the muscle tissue area remains low.

2) VERTICAL CROSS-CUT

Next, we study the power flow on the vertical cross-cut of Laura voxel model, as presented in Fig. 10. The plotted dB range is −65 – 0 dB. The power is evaluated in several different locations (B-G) in terms of different propagation paths through different tissues. Also, in this case, the power is normalized to be 0 dB on the capsule. The power at the location 'B' is −51 dB, which shows quite a significant propagation loss from the capsule. The high power loss can be explained due to small intestine and thick muscle layer, which is points 'A' and 'B'. There is no clear fat layer between the points. Instead, power difference between the locations 'A' and 'C' is minor than power loss difference between the points 'A' and 'B', −38 dB, although the physical distance is equal. The minor power loss difference can be explained by the gap in the muscle layer which provides a partial propagation path though the fat layer between the points 'A' and 'C'.

Physical distance between the locations 'D' and 'E' is also equal, but in this case the power loss difference is 7 dB. 'D' is located in the fat area, whereas 'E' in the intestine area, though with clear fat propagation path between the intestine areas.

These studies give a view how the signal propagates from the implant inside the intestine area. The power flow depends on the antenna radiation pattern but also remarkably on the tissues through which the signal travels. It is also noteworthy that power flow reaches not only the on-body antenna clearly but also the areas largely above and below the antenna, since the signal can propagate easily through the subcutaneous fat layer. This information is useful when designing on-body antenna locations for abdominal implant communication systems, such as capsule endoscope and gastrointestinal activity monitoring systems.

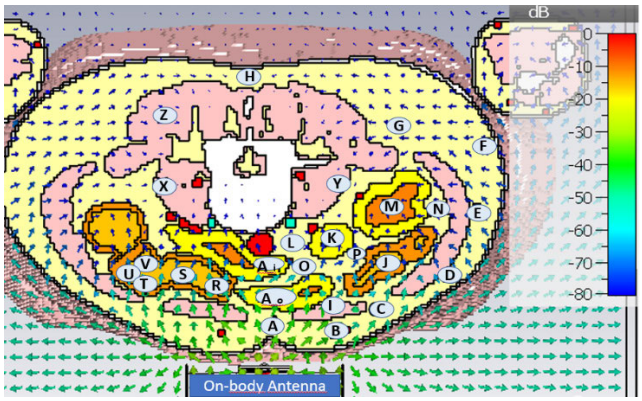

FIGURE 11. Power flow from the on-body antenna at 4 GHz at the locations where the power is evaluated.

Next, we study power flow from the on-body antenna towards the intestine area.

B. ON-BODY ANTENNA POWER FLOW

1) HORIZONTAL CROSS-CUT

Firstly, power flow is studied at 4 GHz for Laura voxel's horizontal cross-cut as presented in Fig. 11. The plotted dB range is −80 to 0 dB where the power is normalized to be 0 dB on the antenna. The power on the skin in this case is −28 dB. Similar power flow figures are presented in [22], but this study covers wider dB range and several different locations within the tissues to enable analysis of the propagation though the visceral fat as well.

As it can be seen from Fig. 11, the signal propagates along the body surface as creeping waves [22] but the part of the signal passes the skin surface and propagates inside the tissues. From the power flow figures one can easily note propagation through the fat layer. For instance, although the on-body antenna is on the navel, the back area can be easily reached within the maximum attenuation of −60 dB as the signal propagates through the subcutaneous fat layer. Instead, the attenuation is strong in the intestine area.

Next, we will investigate the power values in different parts of the subcutaneous fat as well as in the intestine area. Table 3 summarizes the relative power values at $f = 4$ GHz.

Points A - H correspond the power values in the fat layer on the path from the navel to the back. In the location 'A', the power is −35 dB and at H is −105 dB. So the power loss from the antenna on the navel until the middle of the back area is only −70 dB. As the power flow arrows describe, the signal in the fat layer consist of the signal passing through the skin (from creeping waves) as well as the signal propagated through fat layer from the antenna. The power decreases gradually as the distance from the transmitter (Tx) antenna increases. It is noteworthy, that the power is at the points F and G −49 dB and −48.0 dB, respectively. The power is slightly higher at 'G', since there is more power summed from

the larger area of propagation through the fat layer compared to the location 'F', whose power consists mostly the power arriving through the skin.

Next, we compare the power values inside different parts of the intestine and visceral fat area. First, we study the power differences between the points 'A', 'A_o' (outer SI), and 'A_i' (inner SI). One should note that these points are on the central line of the abdomen area where there is no muscle layer and thus propagation is expected to have less losses. Power loss between 'A' and 'A_o' is 10 dB, which is relatively significant since due to the high propagation loss in the SI tissues. At point 'A_i', the power is further decreased even 20 dB.

It is interesting to note how the power is remarkable higher in the points within the visceral fat area compared to the points within the intestine area although the distance from the Tx antenna is the same. For instance, in the furthest location of the small intestine 'M' the power is −99 dB, whereas in the visceral fat location 'N', which is next to M, the power is −85 dB. There are two reasons for such a large difference: location 'M' is in the middle of small intestine and power loss in the small intestine wall and small intestine content is large. Besides, the location 'M' is achieved only from one main direction from the on-body antenna. Although the signal can propagate partially through the visceral fat, it still has to pass thick abdominal muscle layer and other intestine areas before reaching the location 'M'. Instead, the power in the location 'N', which is in the visceral fat area between the intestine and the muscles on the flank, is a sum of power flowing from several different directions: through visceral fat but also through the outer fat.

It is also interesting to note that the power in location 'G' is approximately 20 dB higher than in 'M', although 'M' is clearly closer to the Tx antenna than location 'G'. Similarly, as we compare values in the visceral fat location 'P' and small intestine location 'K', we can note that the power is 5 dB higher in 'P' than in 'K'. At the visceral fat point 'L' and small intestine point 'K', the difference is only 2 dB.

Furthermore, the impact of the fat propagation path on the signal strength can easily be noticed when evaluating power values in the left colon points: 'R', 'S', 'T', and 'U'. At the point 'R', where part of the signal has a direct path from the on-body antenna through the fat layer, the power is −16 dB. Whereas at location 'S', the power level is −32 dB. The loss in the colon tissue is high and, thus, the power difference between the locations 'R' and 'S' is remarkable. At the location 'T', the power is again higher, −22 dB, since the signal can reach the colon from the left side of the abdominal muscle directly through the fat layer. At the locations 'U' and 'V', the power is again significantly lower: −36 dB and −41 dB, respectively.

These power studies verify that the signal propagates with minor losses in the fat tissue. Additionally, the averaged power is higher in the small intestine points, which are in the vicinity of the subcutaneous or visceral fat.

TABLE 4. Power at 4 GHz different points in the abdominal area, horizontal cross-cut.

Subcutaneous fat points	A, A_o, A_i	B	C	D	E	F	G	H
Power [dB]	-35, -45, -67	-36	-49	-66	-74	-80	-79	-105
GI/Visceral fat points	I	J	K	L	M	N	O	P
Power [dB]	-41	-71	-82	-80	-99	-85	-70	-76
Colon/ muscle points	R	S	T	U	V	X	Y	Z
Power [dB]	-46	-63	-53	-67	-72	-132	-136	-121

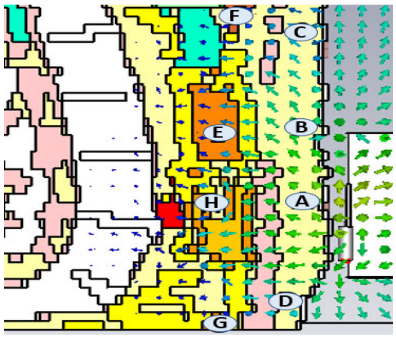

FIGURE 12. Power flow from the on-body antenna at 4 GHz at the locations 'A'-'F'.

2) VERTICAL CROSS-CUT

Next, power flow is studied in the vertical cross-cut of Laura voxel as presented in Fig. 12. Also in this case, plotted dB range is −80 – 0 dB, where the power is normalized to be 0 dB at the antenna. Also in this case, power on the skin is −27 dB.

As one can note, power flow spreads widely in the z-direction (vertically) through the subcutaneous fat layer. Even the lower parts of the stomach as well as lower part of the intestines can be reached within the selected dB range since signal can propagate with low loss through the outer fat layer. Table 4 presents power values in different points of the abdomen area. Locations 'A'-'D' depict power in the subcutaneous fat at different distances from the antenna. The locations 'E'-'H' depict power at different parts of the intestine. The distance between the locations 'A' and 'B' as well as 'A' and 'H' is same, approximately 4.5 cm. As one can note, power loss between locations 'A and 'B' is moderate, only 13 dB, whereas the power loss between locations 'A' and 'H' is significant: 44 dB. As a comparison, power loss between the points 'A' and 'C' is minor, only 36 dB although the distance between these points is approximately 10 cm. This is due to the fact that power loss in the fat tissue is remarkably minor whereas power loss in the intestine tissues (colon, small intestine) is much larger [31]. Naturally, antenna pattern has impact on the power values. However, as shown in [33], this antenna has a clear beam towards intestine areas. The

TABLE 5. Power at 4 GHz at different locations in the abdominal area.

Locations	A	B	C	D	E	F	G	H
Power [dB]	-31	-44	-67	-58	-70	-77	-88	-75

FIGURE 13. The layer model with the fat tunnels on the sides of the antenna substrate.

power loss in the other points of the intestine is moderate: in locations 'E' (SI) and 'F' (the lowest part of the abdomen) loss is 70 dB and 77 dB, respectively. Instead, for the location 'G', the power loss is relatively high, 88 dB.

IV. CHANNEL EVALUATIONS WITH SIMULATIONS

In this section, channel characteristics between the in-body and the on-body antennas are evaluated by simulations using layer models and voxel models described in Section II.

A. LAYER MODEL EVALUATIONS

First, the impact of the fat layer is simulated using layer models: the original layer model with the thickness described in the Section II as well as layer models where the muscle layer is fully or partially (by half) replaced with the fat layer. In the partial replacement case, the border line between the muscle layer and fat layer is in the middle of the antennas. Additionally, the impact of the fat tissue is studied by inserting small fat tunnels through the muscle layer in the vicinity of the antenna substrate, as shown in Fig. 13. The aim of these different layer model versions is to model with very simplified manner different areas in the pork meat pieces in which muscle and fat layers are interlaced: in certain areas, there is basically no muscle layer or very thin one, in certain areas, the muscle layer is partially replaced by fat layer in the close proximity of the antenna. Furthermore, in some areas, there are fat tunnels through the whole meat pieces, which may enhance propagation between the in-body and the on-body antennas. The aim of these layer models studies is to evaluate fat propagation in these different cases, the aim is not to illustrate realistically *Meat1* or *Meat2*.

Firstly, the channel parameters S21 obtained with the original layer model and the modified layer models are studied in Fig. 14a. As one can note, channel attenuation decreases as the amount of fat increases in the model. The S21 is roughly 12 dB at lower level in the original case than in the case where muscle layer is fully replaced with the fat layer. In the case

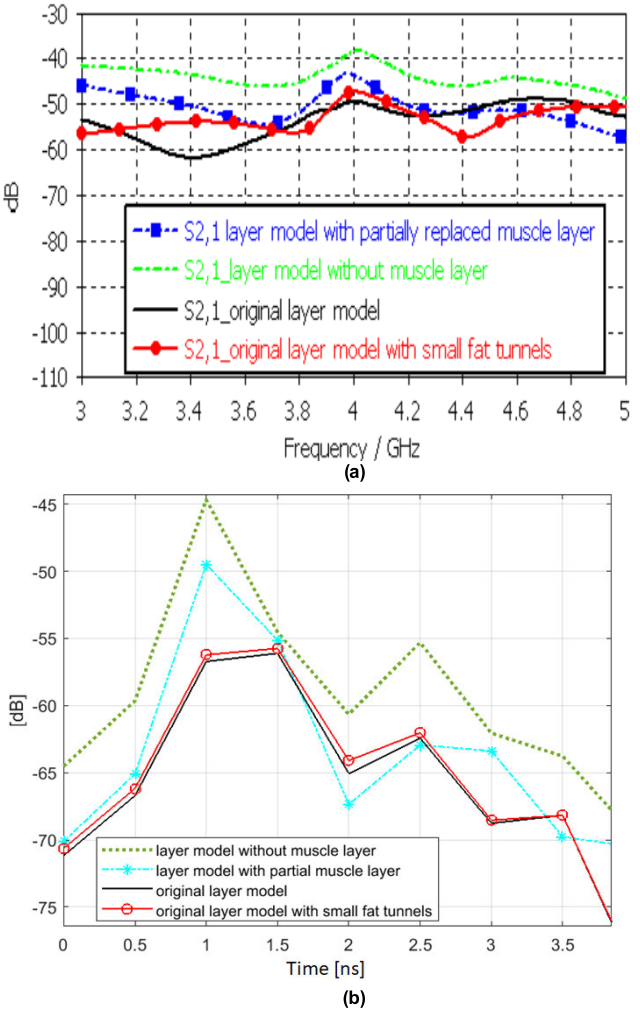

FIGURE 14. a) S21s and b) impulse responses obtained with different layer models variations.

of the layer model where muscle layer is replaced partially with the fat layer, the S21 difference is approximately 2-8 dB within the frequency range of interest. The small fat tunnels improve channel approximately 1-2 dB in the frequency range of interest, except at 3.75 GHz, in which the channel attenuation is slightly stronger in the presence of fat tunnels.

Simulted antenna reflection coefficients are presented in Fig. 1 and thus they are not repeated here.

Next the corresponding channel analysis is done in time domain. The impulse responses (IR) obtained with these layer models are presented in Fig. 14. The presented IRs include impact of Tx and Rx antennas. The IR of the original layer model is presented as solid black line in the figure. It has a relatively wide main peak between 1-1.5 ns, whose level is at highest −56 dB at 1.5 ns. If the muscle layer is replaced with fat tissue, the channel strength increases significantly: approximately 13 dB in the main peak and around 7 dB in the side peaks. Besides, the main peak is clearly narrower reaching highest level at 1 ns. These changes in the IR were expected since the dielectric properties of the fat tissue are remarkably more favorable for propagation than those of the

muscle tissue. The IR obtained using the layer model, where half of the muscle tissue is replaced with the fat tissue has also a narrower main peak which is at the level of −50 dB. This is approximately 7 dB higher than in the original case. Also in this case, there is a peak at 1.5 ns approximately at the same level as in the original case.

Finally, the IR of the layer model with small fat tunnels on the sides of the antenna substrate increases slightly the channel strength, in this case 0.5-1 dB. The impact is assumed to be larger if the fat tunnels are wider and directly below the antenna. This result is used as reference case in Section IV, where measurement results are presented.

As we compare the frequency domain and time domain channel analysis, we can see similar tendency in both cases: replacing muscle tissue by fat tissue totally, partially or even with small tunnels, the channel improves clearly. However, interestingly in certain frequencies or in certain time instants, the channel is found to be stronger in the case of the original layer model. This is assumed to be due to the diffractions from the tissue edges, which in certain areas may affect destructively depending on the antenna radiation pattern. More detail study of this phenomenon is left as future work.

Appendix presents fat propagation studies with the layer models and two different low-UWB on-body antennas having different cavity sizes than the antenna considered in this main text.

Next, we verify the layer model simulation results with propagation path calculations. The basic idea in the propagation path calculations is to calculate propagation time and propagation loss in the tissues for different propagation paths; direct paths as well as the paths which are easiest for the propagation due to more favorable tissues. The propagation paths are determined on the cross-cuts of the voxel models by estimating propagation distances in each tissues for each propagation path. Once the propagation distance and dielectric properties of the tissues are known e.g. from [30], [31], we can calculate propagation time and power loss using Matlab -based planar model propagation as explained in details in [34], [38].

In this layer model study, we calculate power loss and propagation time for the original layer model as well as the layer model in which the muscle layer is replaced by the fat layer. The propagation time and power loss values are presented in Table 6. The layer thicknesses are presented in Table 1 in Section II. According to the calculations, the power difference between the original layer model and the model where muscle layer is replaced with fat layer is 9 dB, which is close to the difference obtained with the simulation results (10 dB). Propagation time difference is 0.15 ns, which differs from the simulations slightly as well.

B. VOXEL MODEL EVALUATIONS

Next, the fat propagation is studied with the channels obtained using CST's voxel models Laura, Donna, and Gustav, who all have different sizes and body constitutions. The frequency and time domain channel characteristics obtained

TABLE 6. Propagation time and power loss with the original layer model and the layer model having muscle layer replaced with fat tissue.

Layer model	Propagation time [ns]	Power loss [dB]
Original layer model	0.93	41
Layer model having muscle layer replaced with fat tissue	0.78	32

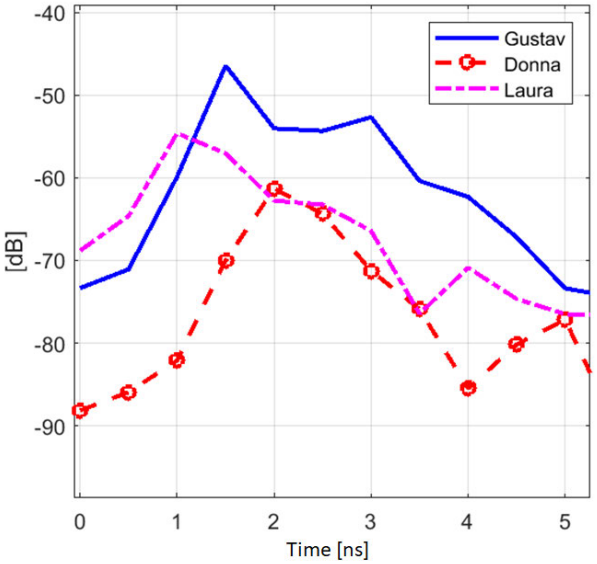

FIGURE 15. Impulse responses obtained with Gustav, Donna, and Laura voxels.

with these antennas and these voxels models have been studied comprehensively in [8]. Thus, we repeat here only the IRs of Gustav, Laura, and Donna voxels in Fig. 15 to enable more detailed study on the impact of the fat on the channel characteristics and ease the comparison with the propagation path calculations.

As one can note, there are significant differences in channel attenuations and propagation times between these different voxel models. The IR's main peak arrives earliest with Laura and latest with Donna, having difference almost 1 ns. Instead, channel is strongest with Gustav model and weakest with Donna, the difference is almost 14 dB. Next, we study the cross-cuts of the voxel models more in detail to understand these differences.

Figs. 16. a-c repeats the cross-cut figure of Gustav, Laura, and Donna, respectively, presented in Figs. 3a-c in Section II, but as zoomed versions with illustrative lines representing two most dominant propagation paths. These paths have been estimated from power flow diagrams. The *direct path*, which corresponds to the shortest physical distance between the capsule and the on-body antenna, is illustrated with an arrow having a solid line. The thicknesses of the tissues as well as calculated propagation time and propagation loss on these propagation paths are listed in the Table 7.

The arrow having dashed line corresponds to the "*fat path*" though the visceral and outer fat tissues avoiding the muscle tissue. The thicknesses of the tissues as well as calculated

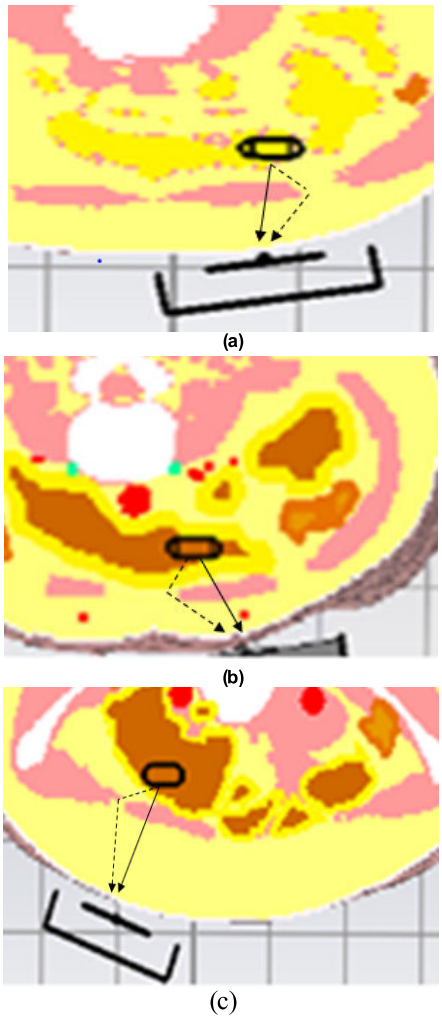

FIGURE 16. The direct path (solid line) and the main fat path (dashed line) on the cross-cuts of a) Gustav, b) Laura, and c) Donna voxels.

propagation time and propagation loss on these propagation paths are listed in the Table 8.

As we compare the results of propagation path calculations for the *direct* path, we can see that propagation time and loss is smallest with Laura-voxel and highest with Donna-voxel. The power loss difference is 5 dB between Laura and Donna, the propagation time difference is 0.36 dB. The results of Gustav are somewhat between those of Laura and Donna. Instead, for the *fat* path, propagation time and loss are clearly smallest with Gustav, even 0.3 ns and 15 dB smaller than that with Donna.

When comparing the IRs obtained with different voxels, one can note that the power loss is smallest with Gustav-voxel, but the propagation time is smallest with Laura-voxel. The reason these differences are that with Gustav, the capsule is located in the very outermost corner of the small intestine which is known to be challenging propagation medium due to its dielectric properties. Hence, the signal prefers a more convenient way to propagate out from the small intestine before reaching the fat layer. Besides, with Gustav model, there is continuous visceral fat layer surrounding abdominal

TABLE 7. Direct propagation path for different voxel models.

Thickness [mm]	Gustav	Donna	Laura
Skin	2	2	2
Outer fat	22	50	15
Muscle	12	9	9
Inner fat	9	4	5
Small intestine	10	10	10
Propagation time [ns]	0.77	0.94	0. 68
Propagation loss [dB]	33	35	30

TABLE 8. Propagation through fat tissues for different voxels.

Thickness [mm]	Gustav	Donna	Laura
Skin	2	2	2
Fat (visceral & outer)	44	75	40
Small intestine	5	10	12
Propagation time [ns]	0.5	0.85	0.63
Propagation loss [dB]	19.7	35	26.4

muscle and SI, which enables propagation through the fat layer in different directions and hence, a larger amount of signals from different directions are summed up in the receiver (Rx). Instead with Laura and especially with Donna, the small intestine is wider in this cross-cut and hence, the access for the surrounding fat tissue in different directions is more challenging.

One should note that these propagation calculations describes propagation only from one horizontal cross-cut. As seen from power flow studies on vertical cross-cuts in Section II, overall power close to the Rx antenna vary significantly depending on the tissues between the capsule and Rx antenna. Thus, the propagation path calculations conducted with the tissue thicknesses at only one horizontal cross-cut does depict the overall propagation between the capsule and the Rx antenna, and hence propagation time do not match completely with the peak locations in the IRs. The better view on the match between the propagation path calculations and simulated IR's would be obtained by studying power flows at different cross-cuts and calculating propagation paths with the tissue thicknesses in these different cross-cut. However, the comparison between the propagation path calculations and simulated IRs is not in the main scope of this study and thus, such extensive power studies at different cross-cuts are left as future's work.

V. CHANNEL EVALUATIONS WITH PORK MEAT MEASUREMENTS

In [32], the author has presented channel evaluations between a in-body and on-body antennas using different pork meat pieces in terms of fat and muscle composition. It was shown that the channel is significantly stronger with the meat pieces where the fat and muscle layers are interlaced compared to the meat piece having distinct muscle and fat layers. In the interlaced model, fat layers passing through muscle layers

FIGURE 17. Additional meat piece set below the original *Meat1* piece. The locations of the loop antenna as well as the fatty area of the *Meat1* are depicted in the figure.

provide easier propagation paths for the signal and thus the channel strength is several dBs higher.

In this study, we further evaluate how the fat layer may ease the propagation through the tissues. Two different pork meat pieces are used as presented in Figs. 6 a-b in Section II. Besides, channel characteristics are evaluated with minced meats having different fat percentages, as presented in Figs. 7c-e to provide insight how even thin fat slices in the meat have affects on the channel strength.

The main focus on this study in on the IEEE802.15.6 standard's mandatory channel 3.75-4.25 GHz but the propagation at lower and higher frequencies is also briefly discussed.

A. IMPACT OF FAT CONNECTIONS

In this study we use same meat tissue as in [32], denoted as *Meat1*, whose thickness is 3 cm. Here we increase the thickness by setting 0.5 cm thick additional meat piece over the original meat piece *Meat1*. The *Meat1* together with additional meat piece is denoted as *Meat1B*, and its thickness is 3.5 cm. This additional piece has several fat stripes, as seen in Fig. 17. As the loop antenna is located in the measurements below *Meat1* and this additional meat piece, these fat stripes are not exactly above the loop antenna but starting from the edges of the antenna as shown in Fig. 17. In the measurements of the original *Meat1*, the loop antenna sides were not touching clearly the fatty areas as seen from Fig. 7a. The fat stripes of the additional pieces connect the loop antenna edges to the fat area of the original piece (marked as a cross in the left side of Fig. 17).

Firstly, the antenna reflection coefficients for the loop antenna (S11) and the on-body antenna (S22) are evaluated in Fig. 18a in the case on *Meat1* and *Meat1B*. As noted from S11 results, the loop antenna operates reasonably within the whole simulated bandwidth 2-10.6 GHz. Instead, the on-body antenna's operational frequency is at 4 GHz as seen from S22 results and as it was designed in [33]. Additionally, the on-body antenna's S22 has a light notch at 9-10 GHz. This paper focuses mostly on the on-body antenna's actual operational bandwidth 3.75-4.25 GHz while discussing briefly the propagation at 9-10 GHz as well.

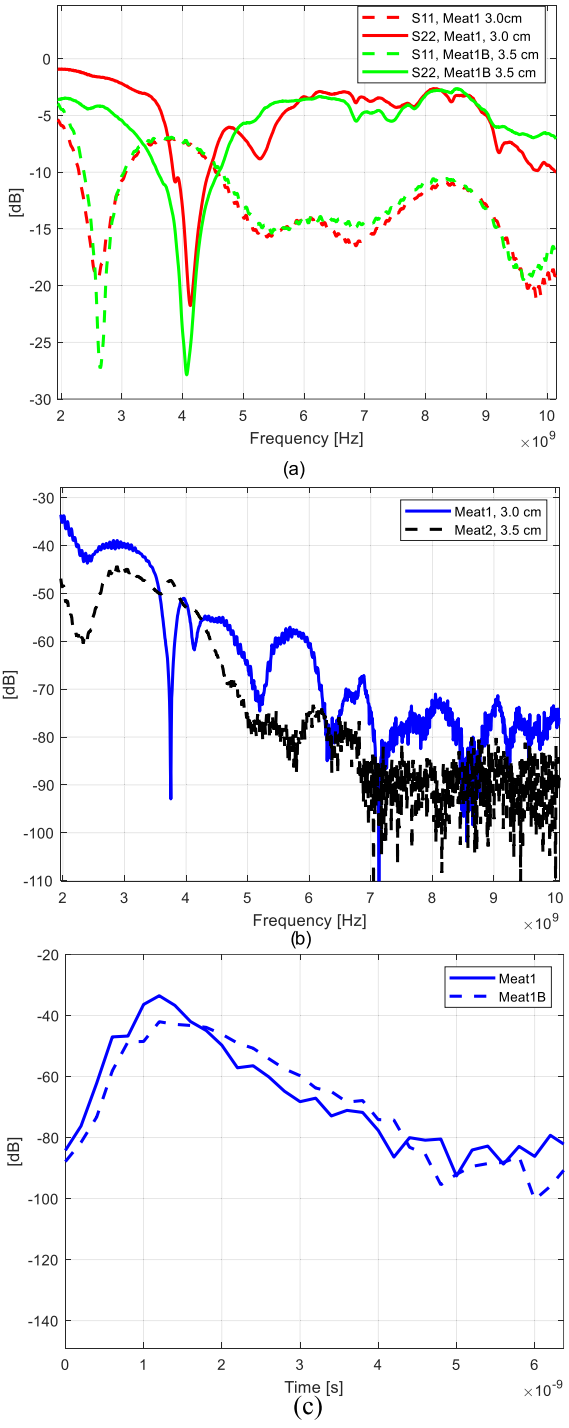

FIGURE 18. a) Measured antenna reflection coefficients for the loop antenna (S11) and the on-body antenna (S22) with *Meat1* and *Meat1B*, b) S21s obtained with *Meat1* and *Meat1B*, c) impulse responses obtained with *Meat 1* and *Meat1B*.

When comparing S11s obtained with *Meat1* and *Meat1B*, one can note that there are only minor changes. The notch at 2.8 GHz is few decibels deeper with *Meat1B*, which however is out of the actual frequency range of interest. At 3.75-4.25 GHz, the loop antenna has similar matching both in the cases of *Meat1* and *Meat1B*. Instead, small changes can be seen in the matching of the on-body antenna, S22.

The antenna matching at the frequency range of interest is slightly better in the case of *Meat1* than in *Meat1B*. One should note that these matching differences in S22 are not due to the additional meat piece itself, since it does not affect on the on-body antenna matching through the meat piece. Instead, the differences are due to the slight unintentional changes in the antenna positioning above the pork skin layer. As discussed e.g. in [38], even the small changes in the antenna positioning or in the antenna-skin distance may impact strongly on the antenna matching.

The frequency and time domain channel characteristics obtained using *Meat1* and *Meat1B* are presented in Figs. 18b-c, respectively. The S21 parameter obtained using *Meat1* seems to fluctuate strongly within the frequency range of interest, whereas the S21 parameter obtained using *Meat1B* is clearly smoother. With *Meat1,* there is also a deep notch at 3.75 GHz, for which S11 and S22 results do not provide explanation. Antenna matching is slightly weaker in the case of *Meat1* than *Meat1B* at 3.75 GHz, but yet very good and hence does not explain the notch. Within the frequency range of interest, the channel attenuation is stronger with *Meat1* than *Meat1B* in the notch area 3.75-3.9 GHz as well as at 4.05-4.25 GHz. Only at 4 GHz, the channel attenuation is minor for *Meat1* than for *Meat1B*. This result is interesting since the overall channel attenuation is expected to be higher with a thicker *Meat1B*.

The channel attenuation is modest also at 2-3.5 GHz, especially in the case of thinner meat piece *Meat1*. One reason for such low channel attenuation is that the loop antenna works well also at this frequency range, as it can be seen from the antenna reflection coefficients S11s presented in Fig. 18a. Instead, the reflection coefficients for the on-body antenna, S22s, show poor operation of the on-body antenna in this frequency range. Despite of that, channel attenuation is modest since in general the propagation loss is clearly milder at lower frequencies [31]. Thus, as the propagation depth is modest, only 3 cm, the channel attenuation can be moderate although the both antennas do not work ideally. However, as the thickness increases, the significance of the directive on-body antenna's good operation increases.

As mentioned earlier, both antennas operate reasonably also at 9-10 GHz. However, the attenuation of the channel is very strong at so high frequencies: approximately at −75 dB with *Meat1*, which is considered slightly above the noise level especially, and −88 dB with *Meat1b,* which is basically at noise level. Thus, such high frequencies could be used only in the in-body communication applications where propagation depth is moderate, depending on the receiver's sensitivity criteria.

In time domain, the main IR peak of the original *Meat1* is at the higher level than that of *Meat1B*. This is natural due to difference in thicknesses. However, one can note that the IR's side peaks are stronger at the time range of 1.8 – 4.5 ns in the case when additional meat piece is included. The reason for this is assumed to be due to the several fat stripes of the additional meat piece which provide smooth connection for the signal to the original meat piece's fatty layers. The signal may propagate partially through fat layers with lower losses and thus the side peaks are clearly at the higher lever. Similar tendency was noted in the simulation results with the layer model having small fat tunnels as presented in Fig. 14: The inclusion of even the small fat tunnels close to the sides of the antenna substrate increased IR's side peak strength slightly. In the case of *Meat1B*, the fat stripes are larger and thus the difference is more noteworthy.

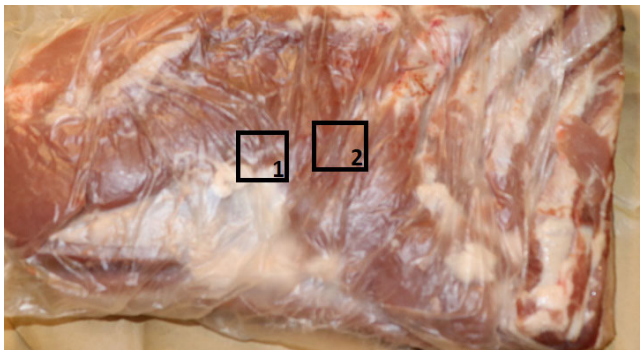

FIGURE 19. Antenna locations in *Meat2*.

B. IMPACT OF ANTENNA LOCATION RESPECT TO THE FAT LAYER

In this study, the impact of the antenna location respect to the fat layer is studied by evaluating the channel characteristics with *Meat2,* which is a large pork meat piece with mostly distinct layers of muscle and fat. Only small and sparsely located ''fat tunnels'' were observed through the meat piece.

The measurements were conducted in two different locations, as presented in Fig. 19. In the first location, denoted as ''Location 1'', the antenna's bottom is connected to the larger fat area which reaches until the lowest edge of the meat piece. In the second location, denoted as ''Location 2'', the loop antenna is located in the middle of the muscle area with only a minor fat connection at the upper corner of the loop antenna. In both cases, the on-body antenna is placed directly above in the loop antenna. In both locations, the thickness of the meat is 3.4 cm.

First, the antenna reflection coefficients S11 and S22 for the loop and the on-body antenna measured in the antenna locations 1 and 2 are studied in Fig. 20a. There are only minor differences in S11s within the frequency range of interest between these antenna locations. Also, the differences in S22 parameters are relatively small. The S11 loop antenna operates reasonably through the whole measured bandwidth whereas the on-body antenna has the main notch around 4 GHz and, also, a minor notch at 9-10 GHz, as in the case of *Meat1* and *Meat1B*.

The frequency and time domain channel characteristics obtained with the antenna locations 1 and 2 are presented in Figs. 20b-c, respectively. In frequency domain, the channel attenuation is found to be maximum 7 dB lower in the location 1 than in the location 2 within the frequency range of interest.

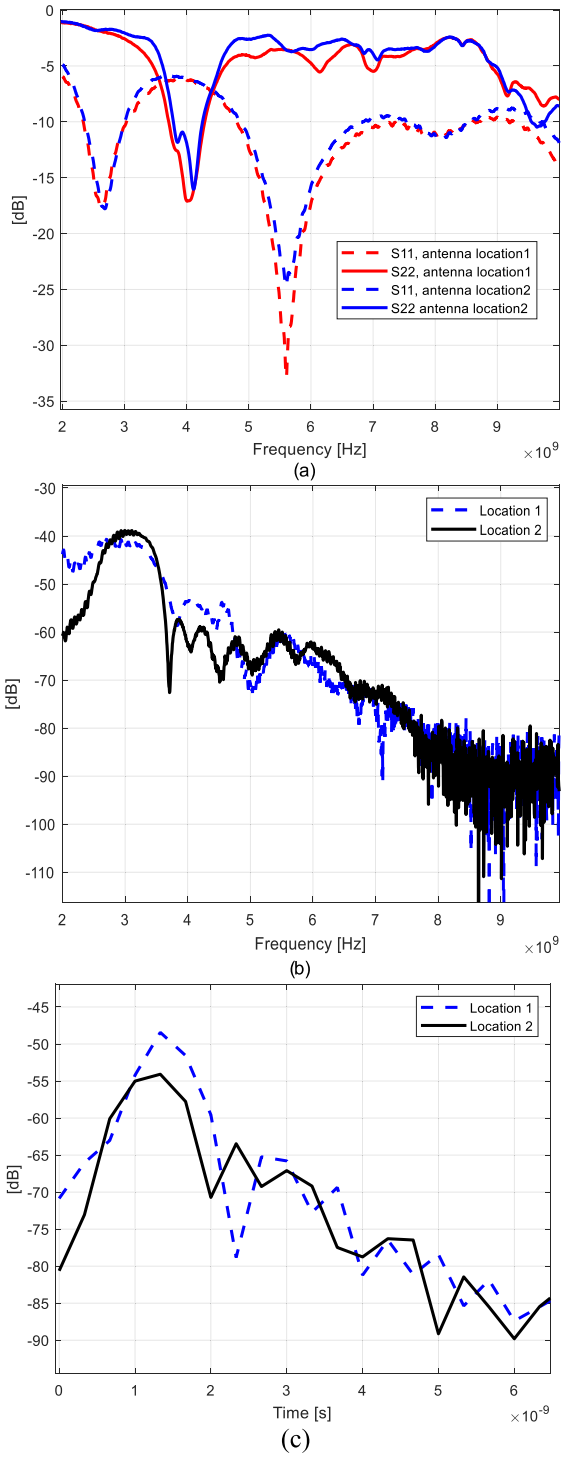

FIGURE 20. a) Antenna reflection coefficients for the loop antenna (S11) and the on-body antenna (S22) measured with *Meat2* at antenna Location1 and Location2, b) S21s obtained at Location1 and Location2, c) impulse responses obtained at Location1 and Location2.

At 3.75 GHz, the attenuation is somewhat same in both antenna locations. Since there are no significant differences in the antenna reflection coefficients measured in the locations 1 and 2 as presented in Fig. 20a, the differences in S21 are related to the propagation differences. At 9-10 GHz, the channel attenuation is found to be excessive: the S21 parameters are at noise level as in the case of *Meat1B*.

In time domain, the difference between the levels of the main peaks is noted to be 6 dB in the favor of Location1. Besides the main peak measured in Location 1 is clearly wider, which is assumed to be due to the wide fat area above the loop antenna providing more lower loss multipath propagation possibilities between the loop antenna and the on-body antenna than in Location2. Furthermore, the wide fat coverage on the bottom edge of the antenna enables smooth connection to different propagation paths through the meat. Moreover, the most of the side peaks are at lower level at the location 2.

Similar phenomenon was also seen in the layer model simulation results presented in Fig. 14, especially in the results where the muscle layer is replaced totally or partially with the fat layer. The increase of the fat tissue does not only increase the IR's peak level but also has impact on the width of the peaks.

C. EVALUATIONS WITH MINCED MEAT HAVING DIFFERENT FAT PERCENTAGES

The results with different pork meat pieces presented in Sections A and B show that uniform and constant "fat tunnels" through the meat's muscle area enhance the propagation. Next, we will study, how small chopped non-uniform fat pieces have impact on the channel attenuation. This study is conducted using minced meat pieces with different fat percentages: 10 %, 15% and 20 %. The minced meat is from beef since pure pork minced meat was not available. Also in this case, the loop antenna and the on-body antennas were set on the below and top of the minced meat pieces.

Firstly, the antenna matching of the loop and on-body antennas measured with different minced meats are studied in Fig. 21a. As one can note, there are slight differences in the reflection coefficients S11s and S22s as measured with different minced meats. The largest difference is in the S22 parameter obtained with minced meat 15% at the frequency range of interest 3.75-4.25 GHz. There is not such a clear notch at 4 GHz as in the cases of minced meats 10% and 20%. However, the antenna matching is still good, clearly below −10 dB. Within the frequency range of interest, the S11 parameters are almost identical for minced meats 10% and 15%. S11 parameter for minced meat 20% is approximately at 2.5 dB lower level than those of 10% and 15%.

The frequency and time domain channel characteristics obtained with these minced meats are presented in Figs. 21a-b, respectively. As one can note, the fat percentage of the minced meat had a clear impact on the channel strength: the higher the fat percentage, the stronger the channel. In frequency domain, the channel attenuation is clearly smallest with 20% minced meat within the frequency range of interest, as well as almost through the whole measured bandwidth. Only at 6-7.5 GHz, the channel attenuation with 20% minced meat is lower than with the other minced

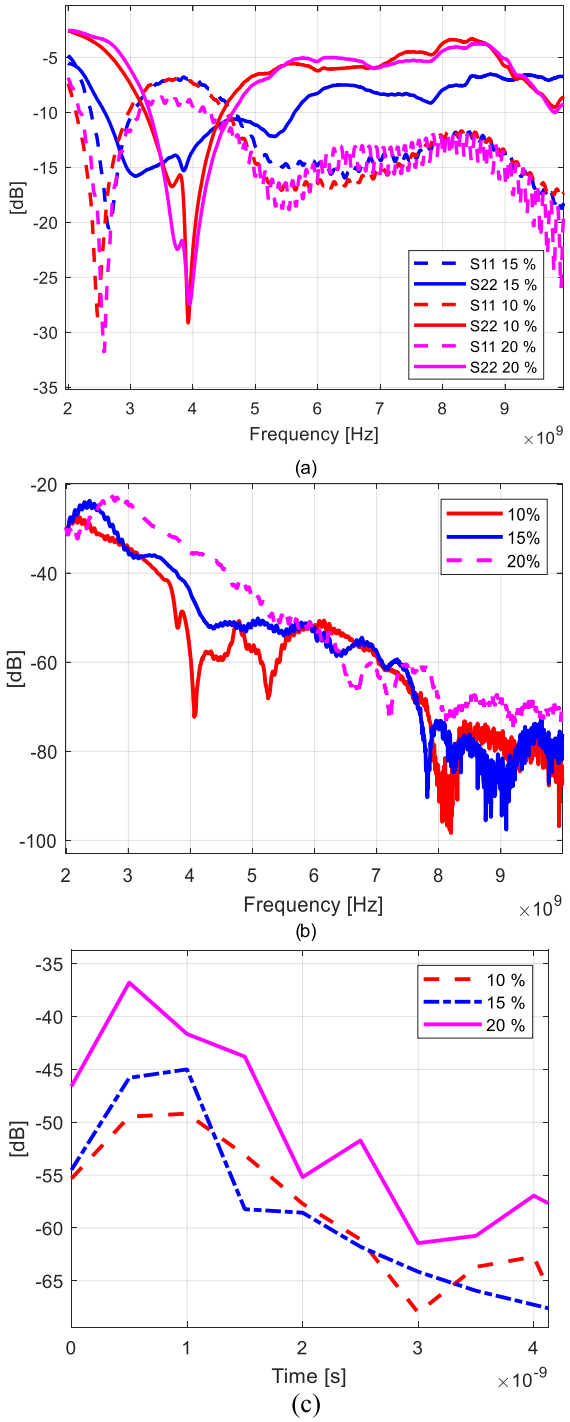

FIGURE 21. a) Measured antenna reflection coefficients for the loop antenna (S11) and the on-body antenna (S22) with different minced meats, b) S21s obtained with different minced meats, c) impulse responses obtained with different minced meats.

meat. The channel attenuation difference between the minced meats of 15% and 20% is remarkable especially in the frequency range of interest: the difference is at highest 24 dB at 4.25 GHz. Instead, the average difference between the minced meats of 10% and 15% is clearly smaller through the whole measured bandwidth than the difference between the minced meats of 15% and 20%. However, at 4.1 GHz, there is a notch in S21 obtained with minced meat 10% which causes approximately 20 dB difference between the minced meats of 10% and 15%.

As expected, the channel attenuation with minced meat 10% is largest within the frequency range of interest, except from 5.5 GHz onwards. However, that frequency range is out of the actual frequency range of interested (3.75-4.25 GHz) and thus left out of comprehensive study in this paper. The differences are only partially explained by the antenna parameters S11 and S22. For instance, difference between S11s of minced meats 10% and 20% is 2.5 dB at 4 GHz whereas the difference in S21s is 35 dB.

Similar tendency can be found in time domain results. When comparing IRs obtained with minced meat having fat percentages of 20% and 15%, one can note that the main peak of the impulse response obtained with 20% minced meat is at 7 dB higher level than in the case of 15% minced meat. Instead, the difference between the main peaks is between the channel obtained using 15% and 10% minced meats is 5 dB. The reason for larger difference between the 20% and 15% cases and 15% and 10% cases is assumed to be due to the larger difference of the fat percentages in reality. When comparing visually the minced meats in Figs. 7c-d, one can note that the difference in respect of the amount of fat is clearly larger between the 10% and 15% cases than between 15% and 20% cases. Additionally, there is variation in the timing of the main peaks: the higher the fat percentage, the earlier is the timing of the main peak.

This phenomenon is clear consequence of the more favorable dielectric properties of fat tissue than of the muscle tissue in terms of propagation loss and also propagation speed. This study shows that even small chopped fat pieces enhance the propagation in the tissues.

VI. DISCUSSION ON THE SIMULATION AND MEASUREMENT RESULTS

The simulation and measurement results as well as propagation path calculation prove the same tendency: the fat is a good propagation medium at 3.75-4.25 GHz since the signal arrives with minor loss and with shorter propagation time if there are fatty areas in the vicinity of the antenna. This was seen both in frequency and time domain results. In frequency domain, the channel attenuation was clearly minor with the simulation models and meat peak pieces with fatty areas, whereas in time domain either the main peak and or side peaks were at higher level. In the layer model simulations, the channel attenuation difference between the most challenging and the easiest cases (i.e. the original layer model and the layer model where muscle layer is replaced with one more fat layer), was noted to be 12 dB in the frequency range of interest. In time domain, the difference between the main peaks was found to be 13 dB and in the side peaks 7 dB. If the muscle layer is only partially replaced with the fat layer (by half), the differences are in frequency and time domain 5 dB and 6 dB, respectively.

These results are in line with the results presented in [32], in which the authors compared the channel characteristics between two different pork meat pieces: the other having separate muscle and fat layers, the other having interlaced muscle and fat layers. In [32], the difference was in frequency domain approximately 11 dB and in time domain (IR main peaks) 10 dB. In the time domain simulation results with partial muscle layer or even with layer model having small fat tunnels, we can see the similar tendency in the IRS' side peaks as in the measurement results with *Meat1* and *Meat2*. Better access to the fatty layer widens the side peaks and may also increase the strength of the peaks. The side peak level was increased clearly in the measurements but less or none in simulation.

Although a similar tendency is clearly seen in the simulation and measurement results, a full correspondence between the simulation and measurement results is not expected in these studies since the simulation models have not been designed to resemble fully *Meat1* or *Meat2* in dimensions or in fat constitutions. Detailed layer model design of meat pieces would require cutting the meat in small pieces to see the structure of the fatty areas or the small fat tunnels in the middle of the meat piece. Instead, the layer model and its variations have been designed so that impact of fat tissue can be studied with simplified examples of different areas in meat pieces.

Additionally, the layer models are designed with the dielectric properties of the human instead of pork. Although the dielectric properties of pork tissue are relatively close to those of humans [40], the differences cause dissimilarities in the channel characteristics as presented in [32].

The propagation studies using layer or voxel model simulations or meat measurements have all their advantages and disadvantages, which have been discussed in detail in [8], [39] and [32], respectively. In abdominal implant communication studies, the layer models have the challenge of too simplified channel characteristics due to lack of realistic propagation environment with visceral fat connections between the outer fat layers [8], [39]. On the other hand, the layer models enable easy changes in the thicknesses of the tissue layers, which is a clear advantage if the impact of the tissue thickness is in the scope of the study. The voxel models provide realistic model for propagation environment, which is essential to obtain realistic channel characteristics between and implant and the on-body antenna, but the voxel models may have challenges with pixelization and excessive simulation times [39].

Pork meat measurements have challenges since the dielectric properties of tissues vary significantly depending on the age and size of the pig, time that has passed after the pig's slaughter, and temperature of the meat during the measurements [40]–[42]. These issues have a clear impact on the channel characteristics [32]. Furthermore, several meat pieces resemble more layer models with separate muscle and fat layers than the voxel models [32]. There may be inaccuracies in the measurement results due to e.g. unintentional differences in the antenna positioning which has impact on antenna matching, as it was also seen in Figs. 18a and 21a. Since the antenna matching effects on the S21 results, it is important that measurement results are verified with simulation results to eliminate the impact of such inaccuracies. Without the simulation results presented with the layer model and its modified versions in Fig. 14, we could not be sure if the differences in the measured S21s are due to the differences in measured antenna reflection coefficients or due to differences in the propagation paths.

Hence, the use of layer and voxel model simulations, meat measurements, analyzing their results carefully while being aware of each model's challenges, as well as reflecting the results with propagation path calculations, provides a comprehensive view on the propagation within the tissues.

The main focus of this paper was on fat propagation studies at 3.75-4.25 GHz since it is the mandatory channel for implant communications in the IEEE802.15.6 standard and the on-body antenna was designed for that frequency range. Besides, propagation on higher frequencies was discussed briefly as well since the on-body antenna was noted to operate also at 9-10 GHz (the loop antenna operated through 2-10 GHz). It was found that in the measurements with *Meat1,* which was the thinner meat piece (3 cm) having interlaced muscle and fat layers, channel attenuation was only 71 dB at 9.1 GHz, whereas with *Meat1B* (3.5 cm) and *Meat2* in both antenna locations (3.4 cm) the attenuation was at noise level at higher frequencies. Presumably, thick fat tunnels through *Meat1* enable propagation with manageable loss even at 9 GHz. This obviously requires that antennas' radiation patterns are favorable and directed towards these fat tunnels. Besides, thickness of the meat piece is critical since with *Meat1B,* the channel attenuation was found to be excessive.

Finally, it was found that channel attenuation is low in many cases also at 2-3 GHz which is not within the on-body antenna's operational frequency range. However, the loop antenna operates also at 2-3 GHz. In general, propagation losses are clearly milder at lower frequencies [31], and thus the channel attenuation can be moderate although the both antennas do not operate ideally. Nevertheless, it was found that if the meat thickness increased from 3.0 cm (*Meat1*) to 3.5 cm (*Meat1B*), the channel attenuation drops significantly at 2-3 GHz. Obviously, the significance of the directive on-body antenna's good operation increases as the propagation depth requirements increases. Furthermore, the location of the antenna respect to the fat layers in *Meat2* has found to have a clear impact on the propagation loss outside the on-body antennas operational frequency ranges as well.

VII. SUMMARY AND CONCLUSION

This paper presented a study on the fat as propagation medium in WBAN abdominal implant communication systems. The study was conducted using different methods and models: with simulations using layer models and CST's anatomical voxel models having different sizes and body constitutions, propagation path calculations, power flow analysis

as well as radio channel measurements with animal meat pieces. The aim was to see whether essentially similar tendencies are observed on the key propagation results obtained with so different methods.

Power flow studies gave a view how the signal propagates from the implant inside the intestine area towards the on-body antenna. The study was repeated also vice versa, i.e. the on-body antenna is the transmitter. The power flow depends on the antenna radiation pattern but also remarkably on the tissues through which the signal travels.

The layer model channel simulation results, both in frequency and time domains, showed that if the propagation through the muscle tissue is even partially replaced with propagation through fat tissue, it improves the channel strength. In the example cases, replacing muscle layer by half with the fat layer, the channel was 5 dB stronger than in the original case. Replacing muscle tissue fully with fat tissue, diminish channel attenuation roughly 10 dB. Even the small fat tunnels close to the edges of the antenna substrate improved channel 1-3 dB.

Simulations with CST's Laura, Donna and Gustav voxels showed that channel attenuation depends not only on the types and thicknesses of the tissues between the Tx and Rx antennas but also how the tissues are located between the Tx and Rx antennas. With Laura voxel, the propagation time was smallest, since the direct propagation distance between the Tx and Rx is smallest. Instead with Gustav-voxel, the propagation loss was smallest due to continuous visceral fat layer surrounding abdominal muscle and SI, which enables larger amount of signals from different directions to be summed up in the receiver. Propagation time and loss was clearly largest with Donna-voxel due to remarkably larger propagation distance and less favorable visceral fat connection than e.g. with Gustav-voxel: level of the main peak of the channel impulse response was even 14 dB lower with Donna than that with Gustav.

Similar tendency could be found with propagation path calculations which were conducted to verify simulation results. However, the propagation path calculations were conducted using the tissue thicknesses at only one horizontal cross-cut and thus, the results do not depict comprehensively the overall propagation between the capsule and the on-body antenna.

Finally, the fat as propagation channel was evaluated with channel measurements using pork meat pieces having different fat and muscle constitution. It was found that antenna location respect to the fat layer has clear impact although the fat tissue is not directly above the in-body antenna. Furthermore, evaluations with minced meats having different fat percentages depicted that even small chopped fat pieces enhance the propagation in the tissues: the higher the fat percentage, the smaller was the channel attenuation.

Appendix presents fat propagation studies with the layer models and two different low-UWB on-body antennas having different cavity sizes than the antenna considered in the main text. It was shown that the larger the cavity, the larger is the impact of the fat layers on the channel attenuation.

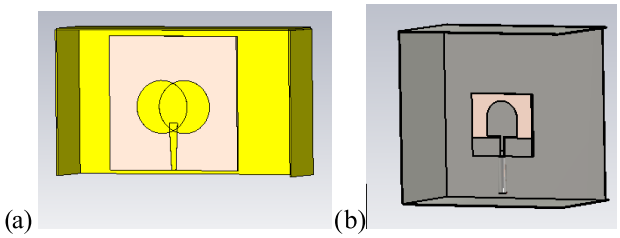

FIGURE 22. a) On-body antenna 2 and b) on-body antenna 3.

VIII. DISCUSSION

The knowledge about the fat as a propagation medium is useful when designing medical monitoring or implant communication systems for UWB range in which propagation loss in the tissues is high. Location of the antennas/sensor nodes for the monitoring devices can be established so that the propagation through the fat layer can be maximized. Appropriate antenna locations can also facilitate that the signal may reach deeper inside the abdominal tissues via subcutaneous and visceral fat, which is useful for the implant communication systems. For instance, in the abdominal area, the propagation depth could be maximized by placing antennas above the central line of the abdomen or between the abdominal muscles from which the connection to visceral fat layer is smoothest. Besides, multiantenna systems design could benefit from the information how the power from the implant may flow through subcutaneous fat relatively far.

Visceral and subcutaneous fat provide a multipath propagation environment in the intestine area. Thus, these kinds of studies require simulations with anatomical voxel models since the layer models lack of the "fat tunnels" between the visceral and subcutaneous fat layers in different directions. However, the use of voxel models has their own challenges, such as small inaccuracies due to pixelization and remarkably increased computational complexity which are discussed more in detail in [39]. Ref. [39] presents also comparison between the on-body channel evaluations using voxel models, different layer models, and human measurements providing also discussion on the advantages and disadvantages of these study methods. In the fat propagation studies, the pixelization of the voxel models may cause some inaccuracies in the power flow studies, since the signal diffractions from the pixelized tissue borders edges differs from those of the smooth borders. Detailed study of the impact of pixelized and smooth tissue borders is left for future's work. Nevertheless, the overall impact of the inaccuracies due to pixelized tissue borders are assumed to be small in fat propagation studies compared to the significant benefits obtained using anatomically realistic models in these evaluations.

The antennas used in this study were selected since they meet frequency band requirements for mandatory channel in WBAN standard. These studies are applicable for other directive, linearly-polarized antennas, as well. At lower frequencies, the dielectric properties of the fat tissue are also more favorable to the propagation than e.g. in muscle layer.

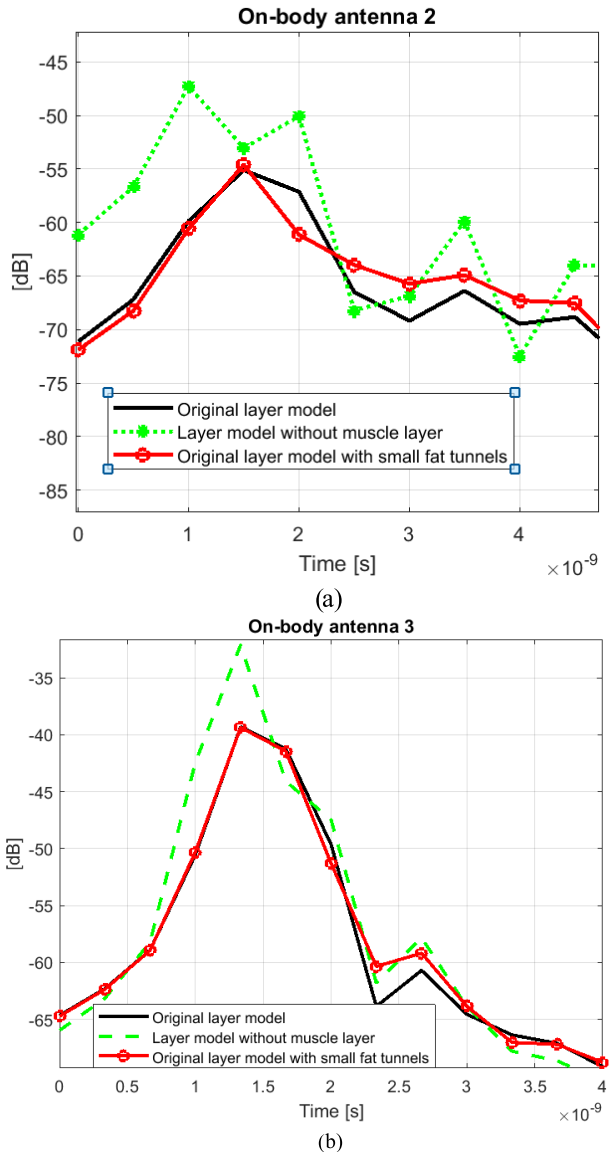

FIGURE 23. **Impulse responses obtained with a) on-body antenna 2 and b) on-body antenna 3 with different layer models.**

However, at lower frequencies, the propagation loss in the tissues is more moderate, and hence the impact of the fat propagation is assumed to be less remarkable since the signal can easily propagate through the muscle layer as well. In general, the lower propagation loss at lower frequencies (even outside the antennas operational frequency) have triggered discussions on the optimal frequency band for implant communications. The lower propagation loss is an obvious advantage but, on the other hand, the use of lower frequencies excludes medical monitoring applications with requirements for high data rate or high resolutions. Besides, implant communications at UWB also provides several advantages for the medical applications, such as low power, low cost and high reliability. Ordinarily, at higher frequency ranges, propagation loss is often considered to be excessively high for implant communications. However, in the fat tissue, the propagation loss is still moderate also at higher frequencies. Thus, as a next step, we will study if also higher frequencies could be suitable for implant communications if the fat as propagation medium could be exploited efficiently

Orientation of the linearly-polarized implant antenna has clear impact on the channel attenuation as presented in capsule endoscope rotation studies in [9]. When the implant antenna is orientated advantageously with respect to the fat paths, it decreases the channel attenuation. Similar tendency is assumed to exist with the loop antenna, which is also linearly-polarized. As future work, we will study this phenomenon more in detail both with linearly and circularly-polarized antennas

There are also several other open study issues to be left as future work. Besides of studying fat as propagation medium with different antennas and antenna, we will evaluate also other frequency ranges already considered applicable for implant communications in different applications. Furthermore, since this study covers only abdominal monitoring applications, we will study, how fat as propagation medium can be exploited in medical monitoring applications on the chest area, e.g. on heart monitoring.

APPENDIX

This Appendix presents fat propagation studies with two other directive on-body antennas designed for in-body communications. The on-body antenna 2, which is presented in Fig. 22 and which was originally introduced in [43], has a larger cavity than the original on-body antenna, with size of x = 96 mm, y = 55 mm, and z = 94 mm, where y is towards the body. On-body antenna 3, which is presented in Fig. 22 b and which was originally introduced in [44], has a smaller cavity, with size of x = 83 mm, y = 19.62 mm, and z = 47.5 mm. The capsule antenna is the same as described in Section II.

The layer models used in this study are 1) the original layer model, presented in Fig. 2, 2) the layer model in which the muscle layer is replaced with one more fat layer, and 3) the layer model in which small fat tunnels are inserted through the muscle layer in the vicinity of the antenna substrate, as shown in Fig. 11.

In this additional study, we evaluated only the time domain channel characteristics for simplicity. The impulse responses obtained with the on-body antenna 2 and 3 in the layer models are presented in Fig. 21a-b, respectively. As it can be noted, the overall tendency in impact of fat layer and small tunnels is similar as in the case of the first on-body antenna. As the muscle layer is replaced with one more fat layer, the levels of the main and side peaks increase. With both antennas, the main peak level increase is approximately 8 dB. Instead, the increase in side peaks is 7 dB with on-body antenna 2 but only 3 dB with on-body antenna 3. The impact of the fat tunnels is also more significant with on-body antenna 2 and on-body antenna 3. The reason for these differences is due to the cavity size: the larger the cavity, the larger is the impact of the fat layers on the channel attenuation. This is quite obvious

since the cavities gather signal from the wider area and hence the overall impact increases.

ACKNOWLEDGMENT

The authors thank Doc. Matti Hämäläinen for the project management. They also thank Dr. Markus Berg for the capsule antenna design and Dr. Marko Sonkki for his participation on the on-body antenna design.

REFERENCES

[1] A. K. Teshome, B. Kibret, and D. T. H. Lai, "A review of implant communication technology in WBAN: Progress and challenges," *IEEE Rev. Biomed. Eng.*, vol. 12, pp. 88–99, 2019.
[2] E. Schires, P. Georgiou, and T. S. Lande, "Vital sign monitoring through the back using an UWB impulse radar with body coupled antennas," *IEEE Trans. Biomed. Circuits Syst.*, vol. 12, no. 2, pp. 292–302, Apr. 2018.
[3] Y. Wei, A. Zahid, H. Heidari, M. Imran, and Q. H. Abbasi, "A compact non-invasive wearablevital signal monitoring system," in *Proc. IEEE Asia Pasific Conf. Postgraduate Res. Microelectron. Electron.*, Oct. 2018, pp. 55–59.
[4] P. Leelatien, K. Ito, K. Saito, M. Sharma, and A. Alomainy, "Channel characteristics and wireless telemetry performance of transplanted organ monitoring system using ultrawideband communication," *IEEE J. Electromagn., RF Microw. Med. Biol.*, vol. 2, no. 2, pp. 94–101, Jun. 2018.
[5] *IEEE Standard for Local and Metropolitan Area Networks_Part 15.6: Wireless Body Area Networks*, IEEE Standard 802.15.6-2012, Feb. 2012, pp. 1–271.
[6] D. R. Cave, S. Hakimian, and K. Patel, "Current controversies concerning capsule endoscopy," *Digestive Diseases Sci.*, vol. 64, no. 11, pp. 3040–3047, Nov. 2019.
[7] C. Kissi, M. Särestöniemi, T. Kumpuniemi, M. Sonkki, S. Myllymäki, M. N. Scrifi, and C. Pomalaza-Raez, "Directive low-band UWB antenna for in-body medical communications," *IEEE Access*, vol. 7, pp. 149026–149038, 2019, doi: 10.1109/ACCESS.2019.2947057.
[8] M. Särestöniemi, C. Pomalaza-Ráez, C. Kissi, M. Berg, M. Hämäläinen, and J. Iinatti, "WBAN channel characteristics between capsule endoscope and receiving directive UWB on-body antennas," *IEEE Access*, vol. 8, pp. 55953–55968, 2020.
[9] M. Särestöniemi, C. Pomalaza-Raez, M. Berg, C. Kissi, M. Hämäläinen, and J. Iinatti, "UWB-WBAN radio channel characteristics between the endoscope capsule and on-body antenna," in *Proc. Int. Conf. Body Area Netw. (BodyNets)*, Oct. 2019, pp. 360–373.
[10] C. Andreu, C. Garcia-Pardo, S. Castello-Palacios, A. Valles-Lluch, and N. Cardona, "Frequency dependence of UWB in-body radio channel characteristics," *IEEE Microw. Wireless Compon. Lett.*, vol. 28, no. 4, pp. 359–361, Apr. 2018.
[11] J.-C. Brumm and G. Bauch, "On the placement of on-body antennas for ultra wideband capsule endoscopy," *IEEE Access*, vol. 5, pp. 10141–10149, 2017.
[12] S. Perez-Simbor, C. Andreu, C. Garcia-Pardo, M. Frasson, and N. Cardona, "UWB path loss models for ingestible devices," *IEEE Trans. Antennas Propag.*, vol. 67, no. 8, pp. 5025–5034, Aug. 2019.
[13] P. A. Floor, R. Chavez-Santiago, T. A. Ramstad, K. Kansanen, A. N. Kim, and I. Balasingham, "Communication aspects for a measurement based UWB in-body to on-body channel," *IEEE Access*, vol. 7, pp. 29425–29440, 2019.
[14] K. M. S. Thotahewa, J.-M. Redoute, and M. R. Yuce, "Propagation, power absorption, and temperature analysis of UWB wireless capsule endoscopy devices operating in the human body," *IEEE Trans. Microw. Theory Techn.*, vol. 63, no. 11, pp. 3823–3833, Nov. 2015.
[15] C. Garcia-Pardo, M. Barbi, S. Perez-Simbor, and N. Cardona, "UWB channel characterization for wireless capsule endoscopy localization," in *Proc. IEEE Int. Conf. Commun. Workshops (ICC Workshops)*, Dublin, Ireland, Jun. 2020, pp. 1–6.
[16] M. Särestöniemi, C. Pomalaza-Raez, M. Berg, C. Kissi, M. Hämäläinen, and J. Iinatti, "In-body power distribution for abdominal monitoring and implant communications systems," in *Proc. 16th Int. Symp. Wireless Commun. Syst. (ISWCS)*, Aug. 2019, pp. 457–462.
[17] A. F. Demir, Q. H. Abbasi, Z. E. Ankarali, A. Alomainy, K. Qaraqe, E. Serpedin, and H. Arslan, "Anatomical region-specific *in vivo* wireless communication channel characterization," *IEEE J. Biomed. Health Inform.*, vol. 21, no. 5, pp. 1254–1262, Sep. 2017.
[18] S. L. Cotton, S. K. Yoo, and W. G. Scanlon, "A measurements based comparison of new and classical models used to characterize fading in body area networks," in *IEEE MTT-S Int. Microw. Symp. Dig.*, London, U.K., Dec. 2014, pp. 1–4.
[19] A. Khaleghi, I. Balasingham, and R. Chavez-Santiago, "Computational study of ultra-wideband wave propagation into the human chest," *IET Microw., Antennas Propag.*, vol. 5, no. 5, p. 559, 2011.
[20] J. Li, Z. Nie, Y. Liu, L. Wang, and Y. Hao, "Characterization of in-body radio channels for wireless implants," *IEEE Sensors J.*, vol. 17, no. 5, pp. 1528–1537, Mar. 2017.
[21] Y. El-Saboni, G. A. Conway, S. L. Cotton, and W. G. Scanlon, "Radiowave propagation characteristics of the intra-body channel at 2.38 GHz," in *Proc. IEEE Int. Conf. Wearable Implantable Body Sensor Netw. (BSN)*, May 2017, pp. 149–152.
[22] M. Särestöniemi, C. Pomalaza-Raez, T. Kumpuniemi, C. Kissi, M. Hämäläinen, and J. Iinatti, "Fat in the abdomen area as a propagation medium in WBAN applications," in *Proc. Int. Conf. Body Area Netw. (BodyNets)*, Oct. 2019, pp. 175–187.
[23] N. B. Asan, D. Noreland, E. Hassan, S. R. M. Shah, A. Rydberg, T. J. Blokhuis, P. Carlsson, T. Voigt, and R. Augustine, "Intra-body microwave communication through adipose tissue," *Healthcare Technol. Lett.*, vol. 4, no. 4, pp. 115–121, Aug. 2017.
[24] N. B. Asan, J. Velander, Y. Redzwan, R. Augustine, E. Hassan, D. Noreland, T. Voigt, and T. J. Blokhuis, "Reliability of the fat tissue channel for intra-body microwave communication," in *Proc. IEEE Conf. Antenna Meas. Appl. (CAMA)*, Dec. 2017, pp. 310–313.
[25] N. Asan, E. Hassan, J. Shah, D. Noreland, T. Blokhuis, E. Wadbro, M. Berggren, T. Voigt, and R. Augustine, "Characterization of the fat channel for intra-body communication at R-band frequencies," *Sensors*, vol. 18, no. 9, p. 2752, Aug. 2018.
[26] N. B. Asan, C. P. Penichet, S. Redzwan Mohd Shah, D. Noreland, E. Hassan, A. Rydberg, T. J. Blokhuis, T. Voigt, and R. Augustine, "Data packet transmission through fat tissue for wireless IntraBody networks," *IEEE J. Electromagn., RF Microw. Med. Biol.*, vol. 1, no. 2, pp. 43–51, Dec. 2017.
[27] N. B. Asan, J. Velander, S. Redzwan, M. Perez, E. Hassan, T. J. Blokhuis, T. Voigt, and R. Augustine, "Effect of thickness inhomogeneity in fat tissue on in-body microwave propagation," in *Proc. IEEE Int. Microw. Biomed. Conf. (IMBioC)*, Jun. 2018, pp. 136–138.
[28] N. B. Asan, S. Redzwan, J. Velander, M. D. Perez, R. Augustine, E. Hassan, T. Voigt, and T. J. Blokhuis, "Effects of blood vessels on fat channel microwave communication," in *Proc. IEEE Conf. Antenna Meas. Appl. (CAMA)*, Sep. 2018, pp. 1–4.
[29] N. B. Asan, E. Hassan, M. D. Perez, S. R. Mohd Shah, J. Velander, T. J. Blokhuis, T. Voigt, and R. Augustine, "Assessment of blood vessel effect on fat-intrabody communication using numerical and ex-vivo models at 2.45 GHz," *IEEE Access*, vol. 7, pp. 89886–89900, 2019.
[30] S. Gabriel, R. W. Lau, and C. Gabriel, "The dielectric properties of biological tissues: II. Measurements in the frequency range 10 Hz to 20 GHz," *Phys. Med. Biol.*, vol. 41, no. 11, pp. 2251–2269, Nov. 1996.
[31] *It'Is Foundation Dielectric Properties For the Materials*. Accessed: Jul. 2017. [Online]. Available: https://www.itis.ethz.ch/virtual-population/tissue-properties/databaseM
[32] M. Särestöniemi, C. Pomalaza-Raez, C. Kissi, and J. Iinatti, "On the UWB in-body propagation measurements using pork meat," in *Proc. Int. Conf. Body Area Netw. (BodyNets)*, 2020, pp. 18–33.
[33] C. Kissi, M. Särestöniemi, C. Pomalaza-Raez, M. Sonkki, and M. N. Srifi, "Low-UWB directive antenna for wireless capsule endoscopy localization," in *Proc. Int. Conf. Body Area Netw. (BodyNets)*, 2018, pp. 431–442.
[34] M. Särestöniemi, C. Pomalaza-Raez, T. Kumpuniemi, M. Hämäläinen, and J. Iinatti, "Measurement data-based study on the intrabody propagation in the presence of the sternotomy wires and aortic valve implant," *IEEE Trans. Antennas Propag.*, vol. 67, no. 8, pp. 4989–5001, Aug. 2019.
[35] M. Särestöniemi, C. Pomalaza-Ráez, Z. Bi, T. Kumpuniemi, C. Kissi, M. Sonkki, M. Hämäläinen, and J. Iinatti, "Comprehensive study on the impact of sternotomy wires on UWB WBAN channel characteristics on the human chest area," *IEEE Access*, vol. 7, pp. 74670–74682, 2019.
[36] T. Tuovinen, K. Y. Yazdandoost, and J. Iinatti, "Comparison of the performance of the two different UWB antennas for the use in WBAN on-body communication," in *Proc. 6th Eur. Conf. Antennas Propag. (EUCAP)*, Mar. 2012, pp. 2271–3374.
[37] *CST Microwave Studio*. Accessed: Jan. 2011. [Online]. Available: http://www.cst.com
[38] S. J. Orfanidis. (2002). *Electromagnetic Waves and Antennas*. Accessed: 2016. [Online]. Available: http://www.ece.rutgers.edu/~orfanidi/ewa/

[39] M. Särestöniemi, C. Kissi, C. M. Pomalaza Raez Hämäläinen, and J. Iinatti, "Measurement and simulation based study on UWB channel characteristics on the abdomen area," in *Proc. 13th Int. Symp. Med. Inf. Commun. Technol. (ISMICT)*, May 2019, pp. 1–6.
[40] M. Ngadi, S. R. S. Dev, V. G. S. Raghavan, and S. Kazemi, "Dielectric properties of pork muscle," *Int. J. Food Properties*, vol. 18, no. 1, pp. 12–20, Jan. 2015.
[41] A. Peyman and C. Gabriel, "Cole—Cole parameters for the dielectric properties of porcine tissues as a function of age at microwave frequencies," *Phys. Med. Biol.*, vol. 55, no. 15, pp. N413–N419, Aug. 2010.
[42] S. Ley, S. Schilling, O. Fiser, J. Vrba, J. Sachs, and M. Helbig, "Ultra-wideband temperature dependent dielectric spectroscopy of porcine tissue and blood in the microwave frequency range," *Sensors*, vol. 19, no. 7, p. 1707, Apr. 2019.
[43] C. Kissi, M. Särestonierni, C. Pomalaza-Raez, M. Sonkki, S. Myllymäki, M. N. Srifi, and H. Jantunen, "High-directivity antenna for low-UWB body area networks applications," in *Proc. Int. Symp. Adv. Electr. Commun. Technol. (ISAECT)*, Nov. 2018, pp. 1–6.
[44] C. Kissi, M. Särestoniemi, T. Kumpuniemi, M. Sonkki, S. Myllymäki, M. N. Srifi, and C. Pomalaza Raez, "Low-UWB receiving antenna for WCE localization," in *Proc. 13th Int. Symp. Med. Inf. Commun. Technol. (ISMICT)*, May 2019, pp. 1–6.

MARIELLA SÄRESTÖNIEMI (Member, IEEE) received the M.Sc., Lic.Tech., and Dr. (Tech) degrees from the University of Oulu, Finland, in 2003, 2005, and 2020, respectively. She is currently a Postdoctoral Researcher with the Centre for Wireless Communications, University of Oulu. Her research interests include medical ICT, wireless body area networks, in-body and on-body propagation, and simulation-based channel modeling and measurements.

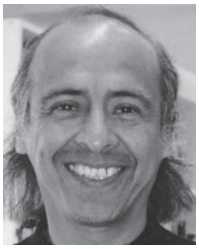

CARLOS POMALAZA-RÁEZ (Senior Member, IEEE) received the B.S.M.E. and B.S.E.E. degrees from the Universidad Nacional de Ingeniería, Lima, Peru, in 1974, and the M.S. and Ph.D. degrees in electrical engineering from Purdue University, West Lafayette, IN, USA, in 1977 and 1980, respectively. He has been a Faculty Member with the University of Limerick, Limerick, Ireland, and Clarkson University, Potsdam, NY, USA. He has also been a Member of the Technical Staff with the Jet Propulsion Laboratory, California Institute of Technology, Pasadena, CA, USA. From 2003 to 2004, he was a Visiting Professor at the Centre of Wireless Communications, University of Oulu, Oulu, Finland, under the auspices of a Nokia-Fulbright Scholar Award. He is currently an Electrical Engineering Professor with Purdue University, Fort Wayne, IN. His research interests include wireless communications networks and signal processing applications.

CHAÏMAÂ KISSI received the degree in engineering from the National School of Applied Sciences, Ibn Tofail University, Kenitra, Morocco, in 2015, where she is currently pursuing the Ph.D. degree with the Electronics and Telecommunication Systems Research Group. Her research interest includes antenna design for medical applications.

JARI IINATTI (Senior Member, IEEE) received the M.Sc., Lic.Tech., and Dr.Tech. degrees in electrical engineering from the University of Oulu, Oulu, Finland, in 1989, 1993, and 1997, respectively. From 1989 to 1997, he was a Research Scientist with the Telecommunication Laboratory, University of Oulu. From 1997 to 2002, he was acting Professor of digital transmission techniques, and a Senior Research Scientist, a Project Manager, and a Research Director with the Center for Wireless Communications, University of Oulu. Since 2002, he has been a Professor of telecommunication theory. He is currently the Head of the Centre for Wireless Communications—Networks and Systems. He has authored about 250 international journal and conference papers, holds six patents. His research interests include future wireless communications systems, transceiver algorithms, wireless body area networks (WBANs), and medical ICT. He has supervised 19 Ph.D. thesis and over 60 master's thesis. He has been a Technical Program Committee (TPC) member in about 25 conferences. He was a TPC Co-Chair in the IEEE PIMRC2006, BodyNets2012 and PIMRC2014, a TPC chair in the ISMICT2007, a General Co-Chair in the ISMICT2011, ISMICT2014 and ISMICT2015, and a TPC Program Track Co-Chair in BodyNets 2012. He was also an Organizer of the FEELIT 2008, the FEELIT2011, the UWBAN2012, and the UWBAN2013. He is Steering Committee Co-Chair of ISMICT series. He is a Co-editor of the book *UWB Theory and Applications* (Wiley & Sons, Ltd., Chichester, U.K., 2004).